

Searching for sterile neutrinos in ice

Soebur Razzaque^{1,*†} and A. Yu. Smirnov^{2,‡}

(1) *College of Science, George Mason University, Fairfax, Virginia 22030, USA*

(2) *The Abdus Salam International Centre for Theoretical Physics, I-34100 Trieste, Italy*

Abstract

Oscillation interpretation of the results from the LSND, MiniBooNE and some other experiments requires existence of sterile neutrino with mass ~ 1 eV and mixing with the active neutrinos $|U_{\mu 0}|^2 \sim (0.02 - 0.04)$. It has been realized some time ago that existence of such a neutrino affects significantly the fluxes of atmospheric neutrinos in the TeV range which can be tested by the IceCube Neutrino Observatory. In view of the first IceCube data release we have revisited the oscillations of high energy atmospheric neutrinos in the presence of one sterile neutrino. Properties of the oscillation probabilities are studied in details for various mixing schemes. The energy spectra and angular distributions of the ν_μ -events have been computed for the simplest ν_s -mass mixing scheme and confronted with the IceCube data. An illustrative statistical analysis of the present data shows that sterile neutrinos with parameters required by LSND/MiniBooNE can be excluded at about 3σ level. The ν_s -flavor mixing scheme, however, can not be ruled out with currently available IceCube data.

*Present address: Space Science Division, U.S. Naval Research Laboratory, 4555 Overlook Ave, SW, Washington, DC 20375, USA

†E-mail: srazzaqu@gmu.edu

‡E-mail: smirnov@ictp.it

1 Introduction

There are several experimental results which could be interpreted as due to oscillations related to existence of sterile neutrinos with mass $m \sim 1$ eV and rather large mixing with ν_μ or/and ν_e . This includes the LSND result [1], the MiniBooNE excess of events in neutrino and antineutrino channels [2], the reactor antineutrino anomaly [3] and the results of the solar calibration experiments [4] (see [5] for recent interpretation). Global analysis of the short-baseline oscillation experiments shows certain consistency of different evidences in the two sterile neutrinos context [6]. Furthermore, the analysis of CMB data indicates an existence of additional radiation in the Universe [7] with sterile neutrino being one of the plausible candidates. The effective number of neutrino species, $N_{\text{eff}} \sim 4-5$, looks preferable. The bound on N_{eff} from the Big Bang Nucleosynthesis (BBN) has been relaxed recently allowing for 1-2 additional neutrinos with the best fit value above 3 species [8].

At the same time, the recent global cosmological analysis which includes the CMB data, large scale structure and BBN results, shows that existence of new neutrino species does not relax significantly the bound on mass of the sterile neutrino [9]. For $\Delta N_{\text{eff}} = 1$ one obtains $m_s < (0.5 - 0.6)$ eV or $\Delta m^2 < (0.25 - 0.36)$ eV² which is smaller than the LSND-required value.

It has been observed some time ago that mixing of sterile neutrinos with $m \sim 1$ eV, and therefore $\Delta m^2 \sim 1$ eV², strongly affects the atmospheric neutrino fluxes in the energy range 500 GeV-few TeV. In this energy range the MSW resonance in matter of the Earth is realized in the $\nu_\mu - \nu_s$ or $\bar{\nu}_\mu - \bar{\nu}_s$ channel [10]. The resonance enhancement of oscillations leads to appearance of a dip in the energy spectrum and to distortion of the angular dependence of tracking (ν_μ -induced) events. These effects can be studied in the IceCube detector [10]. Later in [11] an extended study of the oscillation probabilities has been performed in the presence of one or two sterile neutrinos. As an experimental test it has been proposed to measure the ratio of the tracking and cascade (induced by ν_e) events.

Recently AMANDA [12] and IceCube [13] have published the first high statistics data on the atmospheric neutrinos in the TeV range. (See also results from SuperKamiokande [14]). In this connection we present both analytical and numerical study of properties of the relevant oscillation probabilities for different mixing schemes. We compute the energy spectra and angular distributions of events in IceCube. Results of these computations are confronted with the IceCube data and bounds on the parameters of sterile neutrinos have been obtained. We show that observational results substantially depend in the ν_s -mixing scheme.

The paper is organized as follows. In Sec. 2 we describe the simplest mixing scheme for sterile neutrino (the ν_s -mass mixing) for which dynamics of evolution is reduced to the 2ν -evolution. We obtain the analytical expressions for the oscillation probabilities and present results of numerical computations of the probabilities. In Sec. 3 we study modifications of the atmospheric neutrino fluxes due to mixing with sterile neutrinos. We

compute the number of events for IceCube and confront them with experimental data. In Sec. 4 we perform an illustrative statistical analysis of the data and obtain bounds on the mixing of sterile neutrinos depending on the sterile neutrino mass. In Sec. 5 we study dependence of the probabilities and zenith angle distribution of the ν_μ events on the mixing scheme in the leading order approximation (valid at high energies). Conclusions are given in Sec. 6. In the Appendix we present explicit expressions for the probabilities in the constant density case.

2 Sterile neutrino and conversion probabilities

We will consider mixing of four flavors¹ of neutrinos ($\nu_s, \nu_e, \nu_\mu, \nu_\tau$) which mix in four mass eigenstates ν_i , $i = 0, 1, 2, 3$. We assume the neutrino mass hierarchy: $m_0 \gg m_3, m_2, m_1$, since the opposite situation: $m_3 \approx m_2 \approx m_1 \gg m_0$, with three active neutrinos in the eV range is strongly disfavored by the cosmological data. The mass squared differences equal

$$\Delta m_{03}^2 \equiv (m_0^2 - m_3^2) \sim (0.5 - 3) \text{ eV}^2, \quad \Delta m_{32}^2 \equiv (m_3^2 - m_2^2) \approx 2.5 \cdot 10^{-3} \text{ eV}^2,$$

as is required by the LSND/MiniBooNE and fixed by the atmospheric neutrino results.

As we will show, for high energies ($E > 100 \text{ GeV}$) the electron neutrino mixing can be neglected in the first approximation in consideration of the $\nu_\mu - \bar{\nu}_\mu$ oscillations. Therefore the system is reduced to mixing of the three flavor states $\nu_f^T \equiv (\nu_s, \nu_\tau, \nu_\mu)$ in three mass eigenstates $\nu_{mass}^T \equiv (\nu_0, \nu_3, \nu_2)$ as $\nu_f = U_f \nu_{mass}$, where U_f is the mixing matrix. We will consider the simplest mixing scheme when ν_s mixes in ν_0 and ν_3 with masses m_0 and m_3 only. In this case

$$\nu_f = U_f \nu_{mass} = U_{23} U_\alpha \nu_{mass}. \quad (1)$$

Here U_{23} is the usual 2-3 rotation on the angle $\theta_{23} \sim 45^\circ$ and U_α is the rotation of the mass states ν_0 and ν_3 on the angle α . Explicitly,

$$U_f = U_{23} U_\alpha = \begin{pmatrix} \cos \alpha & \sin \alpha & 0 \\ -\sin \alpha \cos \theta_{23} & \cos \alpha \cos \theta_{23} & \sin \theta_{23} \\ \sin \alpha \sin \theta_{23} & -\cos \alpha \sin \theta_{23} & \cos \theta_{23} \end{pmatrix}. \quad (2)$$

The sterile neutrino mixing is characterized by a single new mixing parameter. In what follows we will refer to (2) as to the ν_s -mass mixing scheme in contrast to the ν_s -flavor-mixing scheme which will be discussed in Sec. 5. The simplest mixing scheme allows us to reduce dynamics of the 3ν -evolution to 2ν -evolution exactly. Other schemes allow to do this only approximately.

According to (2) ν_s mixes with the state

$$\nu'_\tau \equiv \cos \theta_{23} \nu_\tau - \sin \theta_{23} \nu_\mu, \quad (3)$$

¹ ν_s can be treated as the state with zero flavor.

and there is no mixing of ν_s with the orthogonal combination:

$$\nu'_\mu \equiv \cos \theta_{23} \nu_\mu + \sin \theta_{23} \nu_\tau. \quad (4)$$

Thus,

$$\nu_0 = \cos \alpha \nu_s - \sin \alpha \nu'_\tau, \quad \nu_3 = \cos \alpha \nu'_\tau + \sin \alpha \nu_s, \quad \nu_2 = \nu'_\mu.$$

In the first approximation at high energies the dominant effect is due to oscillations driven by the largest mass splitting, Δm_{03}^2 . Therefore the transitions are described by the flavor mixing in the ν_0 state. The corresponding elements of mixing matrix equal

$$U_{s0} = \cos \alpha, \quad U_{\mu 0} = \sin \alpha \sin \theta_{23}, \quad U_{0\tau} = -\sin \alpha \cos \theta_{23}. \quad (5)$$

The mass squared difference Δm_{32}^2 gives sub-leading effects at high energies. But it produces the leading effects at low energies ($E < 0.5$ TeV).

Consider evolution of this system in the propagation basis defined as

$$\tilde{\nu}^T \equiv (\nu_s, \nu'_\tau, \nu'_\mu). \quad (6)$$

It is related to the mass basis as $\tilde{\nu} = U_\alpha \nu_{mass}$, and therefore the evolution equation for $\tilde{\nu}$ reads

$$i \frac{d\tilde{\nu}}{dx} = \tilde{H} \tilde{\nu} = (U_\alpha H_0^{diag} U_\alpha^T + V) \tilde{\nu}. \quad (7)$$

Here $H_0^{diag} \equiv \text{diag}(m_0^2, m_3^2, m_2^2)(2E)^{-1}$, and $V \equiv \text{diag}(-V_\mu, 0, 0)$ is the matrix of the potentials. In V we have subtracted the matrix $V_\mu \mathbf{I}$ proportional to the unit matrix \mathbf{I} . For neutrinos in the electrically neutral medium:

$$V_\mu = V_\tau = -\frac{1}{\sqrt{2}} G_F n_N (1 - Y_e) = -\frac{1}{\sqrt{2}} G_F n_n,$$

where $n_N \equiv \rho/m_N$ is the total number density of nucleons, n_n is the number density of neutrons and Y_e is the number of electrons per nucleon in the medium. In the electrically and isotopically neutral medium $n_n = n_p = n_e$. Therefore $V_\mu = 0.5V_e$, where V_e is the difference of potentials for the $\nu_e - \nu_\mu$ system. For antineutrinos: $\bar{V}_\mu = -V_\mu$. Explicitly the Hamiltonian is given by

$$\tilde{H} = \begin{pmatrix} \frac{\Delta m_{03}^2}{2E} \cos^2 \alpha - V_\mu & -\frac{\Delta m_{03}^2}{4E} \sin 2\alpha & 0 \\ -\frac{\Delta m_{03}^2}{4E} \sin 2\alpha & -\frac{\Delta m_{03}^2}{2E} \sin^2 \alpha & 0 \\ 0 & 0 & -\frac{\Delta m_{32}^2}{2E} \end{pmatrix}. \quad (8)$$

Here again we have subtracted the matrix proportional to the unit matrix $(m_3^2/2E)\mathbf{I}$.

The MSW-resonance condition reads

$$\frac{\Delta m_{03}^2}{2E} \cos 2\alpha = V_\mu,$$

and since $V_\mu < 0$ the resonance is realized in the antineutrino channel. The resonance energy $E \sim (2 - 5)$ TeV ($\Delta m_{03}^2/1\text{eV}^2$), (see the level crossing scheme in [16]). The state ν'_μ decouples and is not affected by matter. It evolves independently as

$$A_{\mu'\mu'} = e^{i\phi_{32}}, \quad \phi_{32} = \frac{\Delta m_{32}^2 x}{2E}. \quad (9)$$

As follows from the form of the Hamiltonian (8) the evolution matrix (matrix of amplitudes) in the propagation basis can be written as

$$\tilde{S} = \begin{pmatrix} A_{ss} & A_{s\tau'} & 0 \\ A_{\tau's} & A_{\tau'\tau'} & 0 \\ 0 & 0 & A_{\mu'\mu'} \end{pmatrix} \quad (10)$$

(no ν'_μ -transitions). From unitarity of \tilde{S} we have:

$$|A_{ss}|^2 + |A_{s\tau'}|^2 = 1, \quad |A_{\tau's}|^2 + |A_{\tau'\tau'}|^2 = 1, \quad |A_{\mu'\mu'}|^2 = 1. \quad (11)$$

According to (3) and (4) the states of the propagation basis $\tilde{\nu}$ are related to the flavor states ν_f as

$$\tilde{\nu} = U_{23}^T \nu_f. \quad (12)$$

Therefore the S matrix in the flavor basis ν_f is

$$S = U_{23} \tilde{S} U_{23}^T.$$

Using (12) and (10) we obtain

$$S = \begin{pmatrix} A_{ss} & \cos \theta_{23} A_{s\tau'} & -\sin \theta_{23} A_{s\tau'} \\ \cos \theta_{23} A_{\tau's} & \cos^2 \theta_{23} A_{\tau'\tau'} + \sin^2 \theta_{23} A_{\mu'\mu'} & -\sin \theta_{23} \cos \theta_{23} (A_{\tau'\tau'} - A_{\mu'\mu'}) \\ -\sin \theta_{23} A_{\tau's} & -\sin \theta_{23} \cos \theta_{23} (A_{\tau'\tau'} - A_{\mu'\mu'}) & \sin^2 \theta_{23} A_{\tau'\tau'} + \cos^2 \theta_{23} A_{\mu'\mu'} \end{pmatrix}. \quad (13)$$

Moduli squared of the elements of this matrix give the corresponding oscillation probabilities. In particular, the $\nu_\mu - \nu_\mu$ survival probability, $P_{\mu\mu}$, equals

$$P_{\mu\mu} = \left| \sin^2 \theta_{23} A_{\tau'\tau'} + \cos^2 \theta_{23} A_{\mu'\mu'} \right|^2, \quad (14)$$

and the other oscillation probabilities with participation of ν_μ are

$$\begin{aligned} P_{\mu s} &= \sin^2 \theta_{23} |A_{\tau's}|^2 = \sin^2 \theta_{23} (1 - |A_{\tau'\tau'}|^2), \\ P_{\mu\tau} &= \sin^2 \theta_{23} \cos^2 \theta_{23} |A_{\tau'\tau'} - A_{\mu'\mu'}|^2. \end{aligned} \quad (15)$$

These probabilities satisfy the unitarity condition: $P_{\mu s} + P_{\mu\tau} + P_{\mu\mu} = 1$. Notice that when $A_{\tau'\tau'} = -A_{\mu'\mu'}$, the transition probability $P_{\mu\tau} = P_{\mu\tau}^{max} = \sin^2 2\theta_{23}$. In this case $P_{\mu\mu} =$

$\cos^2 2\theta_{23}$. Then for maximal 2-3 mixing we have $P_{\mu\mu} = 0$ and $P_{\mu\tau} = 1$, and correspondingly, $P_{\mu s} = 0$.

Consider properties of the survival probabilities in the neutrino and antineutrino channels. Using (9) and (14) we obtain

$$\begin{aligned} P_{\mu\mu} &= \left| \sin^2 \theta_{23} A_{\tau'\tau'} + \cos^2 \theta_{23} e^{i\phi_{32}} \right|^2 \\ &= \sin^4 \theta_{23} P_{\tau'\tau'} + 2 \sin^2 \theta_{23} \cos^2 \theta_{23} \operatorname{Re} \left(e^{-i\phi_{32}} A_{\tau'\tau'} \right) + \cos^4 \theta_{23}, \end{aligned} \quad (16)$$

where $P_{\tau'\tau'} = |A_{\tau'\tau'}|^2$ is the $\nu'_\tau - \nu'_\tau$ survival probability. For antineutrinos we have $A_{\tau'\tau'} \rightarrow \bar{A}_{\tau'\tau'} = A_{\tau'\tau'}(V_\mu \rightarrow -V_\mu)$. For $E \gtrsim 1$ TeV the phase ϕ_{32} is small, $< 3^\circ - 4^\circ$, so that in the lowest approximation

$$P_{\mu\mu} \approx \sin^4 \theta_{23} P_{\tau'\tau'} + 2 \sin^2 \theta_{23} \cos^2 \theta_{23} \operatorname{Re} (A_{\tau'\tau'}) + \cos^4 \theta_{23}. \quad (17)$$

However, the phase ϕ_{32} can not be neglected at low energies, $E \lesssim 0.5$ TeV. Explicit analytic expression for the amplitude $A_{\tau'\tau'}$ is given in the Appendix. In the absence of mixing with sterile neutrino one has $\alpha = 0$, $A_{\tau'\tau'} = 1$, and consequently (16) is reduced to usual vacuum oscillation probability due to the 2-3 mixing and 2-3 mass splitting.

In Fig. 1 we show the probability $\bar{P}_{\mu\mu}$ as a function of neutrino energy for different values of the zenith angle (θ_z) and the oscillation parameters. (In our computations we use the PREM model for the Earth density profile [17].) The typical energy-dependent feature of $\bar{P}_{\mu\mu}$ is the resonance dip in the range determined by the resonance energies in the core and in the mantle. For $|\cos \theta_z| < 0.82$ there is a single dip at $E \sim E_R \sim 4$ TeV which corresponds to the MSW resonance in the mantle of the Earth. For $|\cos \theta_z| > 0.82$ (core crossing trajectories) the dependence of the probability on E is more complicated. The dip between the resonance energies in the core and mantle is due to the parametric enhancement of oscillations, *i.e.* due to an interplay between the oscillation effects in three layers with nearly constant density (mantle-core-mantle) [18]. The width of this dip is larger than the width of the MSW dip in constant density medium. There is also the parametric enhancement of the oscillations at energies above the resonance energy in the mantle [18].

For the $\nu-$ (non-resonance) channel, the peaks are absent (see Fig. 2), but another feature related to the matter effect is realized: enhanced $\mu - \tau$ transition at low ($E < 0.5$ TeV) energies. The survival probability decreases with energy in contrast to the $\bar{\nu}$ channel where $\bar{P}_{\mu\mu}$ increases with energy. The reason can be understood from consideration in the case of constant density (Appendix). At energies below 0.5 TeV the oscillations induced by the 2-3 mixing and mass splitting become important. The dependence of probabilities on energy is given by the oscillatory curve with low frequency in the energy scale and the depth $\sin^2 2\theta_{23} \approx 1$ (see analytic expression in (51)). This curve is modulated by high frequency oscillations driven by Δm_{03}^2 with small depth. At low energies the phase of the low frequency oscillations is given (see (52) in the Appendix) by

$$\phi_2 \approx \frac{1}{2} \left(H_{2m} + \frac{\Delta m_{32}^2}{2E} \right) x \approx \frac{1}{2} \left(\pm |V_\mu| \sin^2 \alpha + \frac{\Delta m_{32}^2}{2E} \right) x,$$

where in last expression the first term is due to the matter effect; the plus sign corresponds to neutrinos and the minus sign to antineutrinos (according to (48), $H_{2m} \sim -V_\mu \sin^2 \alpha$). In the energy interval (0.1 – 0.5) TeV the two contributions are comparable. Thus, the matter effect produces an opposite change of the phase velocity: increasing the velocity in the neutrino channel and decreasing it in the antineutrino channel. Consequently the oscillations due to the 2-3 mass splitting and 2-3 mixing develop in the ν -channel at higher energies. Notice that the phase shift is proportional to $\sin^2 \alpha$, and at low energies $\alpha_m \approx \alpha$ (see Fig. 2, the upper panel).

Let us consider more general situation when ν_s mixes also in the ν_2 state. We introduce an additional rotation U_γ in the ν_3 - ν_2 subspace, so that the propagation basis becomes: $\tilde{\nu} = U_\alpha U_\gamma \nu_{mass}$. Explicitly the mixing matrix in the propagation basis becomes

$$\tilde{U}_f = U_\alpha U_\gamma = \begin{pmatrix} c_\alpha & s_\alpha c_\gamma & s_\alpha s_\gamma \\ -s_\alpha & c_\alpha c_\gamma & c_\alpha s_\gamma \\ 0 & -s_\gamma & c_\gamma \end{pmatrix}. \quad (18)$$

Here $s_\gamma \equiv \sin \gamma$, $c_\gamma \equiv \cos \gamma$, *etc.*. Now ν_s mixes in all three mass eigenstates:

$$\nu_s = c_\alpha \nu_0 + s_\alpha (c_\gamma \nu_3 + s_\gamma \nu_2).$$

The Hamiltonian in the propagation basis equals $\tilde{H}_{\alpha\gamma} = U_\alpha U_\gamma H^{diag} U_\gamma^T U_\alpha^T$, and it can be represented as

$$\tilde{H}_{\alpha\gamma} = \tilde{H} + s_\gamma \frac{\Delta m_{32}^2}{2E} \begin{pmatrix} -s_\alpha^2 s_\gamma & -s_\alpha c_\alpha s_\gamma & -s_\alpha c_\gamma \\ \dots & -c_\alpha^2 s_\gamma & -c_\alpha c_\gamma \\ \dots & \dots & s_\gamma \end{pmatrix}, \quad (19)$$

where \tilde{H} is the Hamiltonian without U_γ rotation (8). The correction is proportional to a small quantity $s_\gamma \frac{\Delta m_{32}^2}{2E}$ which produces even smaller (suppressed by s_γ) phase than ϕ_{32} considered in the simplest case above. So, the effects of ν_s mixing in ν_2 can be neglected in the first approximation.

The mixing matrix in the flavor basis is given by $U_f = U_{23} U_\alpha U_\gamma$. The elements of this matrix which describe oscillations with large mass split Δm_{03}^2 (dominant at high energies) are the same as in our simplest mixing case (5). They do not depend on γ .

In what follows we present predictions for IceCube in the simplest ν_s -mass mixing case. Consideration of the ν_s -flavor mixing schemes is given in Sec. 5, where we show that, in fact, the probabilities and observables substantially depend on the mixing scheme.

3 Fluxes and numbers of events

The ν_μ -flux at the detector equals

$$\Phi_\mu = \Phi_\mu^0 P_{\mu\mu} + \Phi_e^0 P_{e\mu} \approx \Phi_\mu^0 P_{\mu\mu}, \quad (20)$$

where Φ_μ^0 and Φ_e^0 are the original fluxes of ν_μ and ν_e without oscillations. Similar expression holds for the antineutrinos. The effect of $\nu_e \rightarrow \nu_\mu$ oscillations can be neglected (the last equality in (20)). The reason is two fold: at high energies $\Phi_\mu^0 \gg \Phi_e^0$, with ratio $r \equiv \Phi_\mu^0/\Phi_e^0 > 20$ for $E \sim 1$ TeV. Furthermore, the transition probability $P_{e\mu} \ll 1$ and ν_e can be mostly converted to ν_s .

Let us consider ν_e oscillations in some details. At high energies the mixing of ν_e and ν'_μ is strongly suppressed: $\sin^2 2\theta_{12}(E_{12}^R/E)^2$, where $E_{12}^R \sim 0.1$ GeV is the resonance energy associated to the ‘‘solar’’ mass splitting Δm_{21}^2 . The $\nu_e - \nu'_\tau$ mixing is absent in the limit $\theta_{13} = 0$, but if non-zero, the 1-3 mixing in matter is also suppressed in the TeV energy range as $\sim \sin^2 2\theta_{13}(E_{13}^R/E)^2$, where $E_{13}^R \approx 6$ GeV is the energy of 1-3 resonance. Consider whole 4ν -scheme with ν_e admixture, U_{e0} , in the state ν_0 . Since for the ν_e potential we have $V_e \approx -V_\mu$ in the isotopically neutral medium, the $\nu_e - \nu_s$ level crossing is in the neutrino channel. The corresponding resonance energy $E_{es}^R \approx E_{\mu s}^R$. The depth of $\nu_e - \nu_\mu$ oscillations driven by Δm_{01}^2 equals

$$D_{e\mu} \approx 4|U_{e0}^m|^2|U_{\mu 0}^m|^2, \quad (21)$$

where U_{e0}^m and $U_{\mu 0}^m$ are the mixing parameters in matter. In vacuum: $D_{e\mu} = \sin^2 2\theta_{\text{LSND}} \sim 3 \cdot 10^{-3}$. The mixing and the depth can be enhanced in resonances. In the $\bar{\nu}_\mu - \bar{\nu}_s$ resonance the $\bar{\nu}_\mu$ -mixing is enhanced, $|U_{\mu 0}^m|^2 \sim 1/2$, whereas the ν_e -mixing is suppressed: $|U_{e0}^m|^2 \sim |U_{e0}|^2/4$. As a result, $D_{e\mu} \approx |U_{e0}|^2/2 \lesssim 0.02$. In the $\nu_e - \nu_s$ resonance, inversely, the $\bar{\nu}_\mu$ -mixing is suppressed $|U_{\mu 0}^m|^2 \sim |U_{\mu 0}|^2/4$, and ν_e -mixing is enhanced $|U_{e0}^m|^2 = 1/2$. So that the depth of oscillations equals $D_{e\mu} \approx |U_{\mu 0}|^2/2 \lesssim 0.02$. Therefore $P_{e\mu} \lesssim 0.02$, and the contribution of the original ν_e flux to ν_μ flux at a detector, $P_{e\mu}r$, is smaller than 10^{-3} .

The rate of ν_μ events in a detector such as IceCube is given by

$$N = \int dE \int d\Omega \left[\Phi_\mu(E, \theta_z) A_{\text{eff}}(E, \theta_z) + \bar{\Phi}_\mu(E, \theta_z) \bar{A}_{\text{eff}}(E, \theta_z) \right], \quad (22)$$

with the appropriate integrations over the neutrino energy and solid angle. Additional contribution to the muon events comes from the $\nu_\mu \rightarrow \nu_\tau$ oscillations, producing a flux $\Phi_\tau = \Phi_\mu^0 P_{\mu\tau}$ at the detector. The tau lepton from ν_τ interaction has $\approx 18\%$ probability to decay into muon, which is then recorded as a ν_μ event. The ν_τ energy, however, needs to be ~ 2.5 times higher than the ν_μ energy to produce muon tracks of the same energy in the detector. Notice that in the ν_s -mass mixing scheme ν_τ 's appear in the ν_μ oscillation dip, but this will lead to additional events at low energies. In other mixing schemes ν_μ 's are transformed mainly into ν_s 's, and production of ν_τ is suppressed.

In (22) A_{eff} and \bar{A}_{eff} are the effective areas of the detector for ν and $\bar{\nu}$. They are given by the effective volume V_{eff} from which the events (muons) are collected with an efficiency of detection ϵ_{det} as

$$A_{\text{eff}} \sim V_{\text{eff}} n_N \sigma_{\nu N} \epsilon_{\text{det}}.$$

Here n_N is the number density of nucleons in the surrounding medium and $\sigma_{\nu N}$ is the neutrino-nucleon charge-current cross section. In turn, V_{eff} is determined by the geometry

of the detector and the muon range R_μ : $V_{\text{eff}} \propto R_\mu^3$. The range can be estimated as

$$R_\mu = \frac{1}{b} \ln \frac{a + bE_\nu(1 - \langle y \rangle)}{a + bE_{\mu,\text{min}}}.$$

where $a = 0.24 \text{ GeV m}^{-1}$, $b = 3.3 \cdot 10^{-4} \text{ m}^{-1}$, $\langle y \rangle$ is the mean inelasticity and $E_{\mu,\text{min}}$ is the minimum muon energy for detection. At low energies $R_\mu \propto E_\mu$ and at $E \sim 1 \text{ TeV}$ the linear increase of R_μ changes to the logarithmic one (see [13] for details). Since, usually the data are presented using energy bins of equal size in the *log*-scale, the relevant quantity which determines the number of events in a given energy bin is $N_E = A_{\text{eff}} E \Phi_\nu$ (where the E originates from the Jacobian). The differential neutrino flux decreases as $\Phi_\nu \propto E^{-3.7}$, and therefore at low energies N_E increases as $N_E \propto E^{1.3}$. It reaches maximum at $E \sim 0.7 \text{ TeV}$ and then decreases since V_{eff} has only logarithmic increase. The median energy interval $E = (0.15 - 2.3) \text{ TeV}$ is determined by a condition $N_E \geq 0.5 N_E^{\text{max}}$. This interval includes the region of dips in the oscillation probability and therefore IceCube is well optimized to search for sterile neutrinos with $\Delta m^2 = (0.5 - 2) \text{ eV}^2$. The described dependence of N_E on energy allows one to understand various features of the predicted effects.

The effective area is also given by

$$A_{\text{eff}} = A_{\text{det}} S_{\text{Earth}}(E_\nu, \theta_z) P_{\text{int}}(E_\nu),$$

where A_{det} is the geometrical area of the detector, S_{Earth} is the survival probability of neutrino passing through the Earth at a given trajectory and P_{int} is the charged current neutrino-nucleon interaction probability in the vicinity of the detector. The survival probability is given by

$$S_{\text{Earth}}(E_\nu, \theta_z) = \exp \left[-N_A \sigma_{\text{tot}}(E_\nu) \int_0^L \rho(\theta_z, l) dl \right],$$

where $L = 2R_{\text{Earth}} \cos \theta_z$ is the length of the trajectory, $\rho(\theta_z, l)$ is the matter density at a distance l along the trajectory and σ_{tot} is the total neutrino cross-section. For $E \lesssim 10 \text{ TeV}$, $S_{\text{Earth}} \sim 1$. The interaction probability is given by

$$P_{\text{int}}(E_\nu) = N_A \sigma_{\nu N}(E_\nu) \langle R(E_\nu, E_{\mu,\text{min}}) \rangle,$$

where $\langle R(E_\nu, E_{\mu,\text{min}}) \rangle$ is the average muon range in the medium and N_A is the Avogadro's number.

In Figs. 3 and 4 we show the sum of the ν_μ and $\bar{\nu}_\mu$ energy spectra integrated over the solid angle for the ν_s -mass mixing scheme. An estimation of the size of the oscillation effects is rather easy: maximal, $\approx 100\%$, effect is for $\bar{\nu}$ in the resonance range; summation with ν (whose flux is about 1.4 times larger) gives 40% effect; averaging over the zenith angle from 180° to 90° produces another factor $\sim 1/2$, and therefore one arrives at the maximal $\sim 20\%$ suppression in the dip. Relative effect increases with narrowing the integration

region around vertical direction (see Fig. 5). Now the maximal effect can reach 40% and further enhancement would require experimental separation of neutrino and antineutrino signals. With increase of Δm_{03}^2 the dip shifts to high energies as $E \propto \Delta m_{03}^2$. Increase of the size of the dip with $\sin^2 \alpha$ is more complicated. Suppression effect extends to low energies due to oscillations in the ν - channel driven by the 2-3 mixing.

We also compare the predicted neutrino energy spectra in Figs. 3 and 4 with the “un-folded” energy spectra reconstructed by IceCube [13]. Presently, this comparison can be used for illustration only since reconstruction of the unfolded spectra implies significant smearing and in general is not sensitive to the spectral distortion in small energy intervals. Notice, however, that the size of the dip in the energy scale is larger than the size of the bin of the reconstructed spectrum. To have better sensitivity to the distortion one can further decrease the size of the bin.

According to the Fig. 22 of [13] the statistical error in the relevant energy range is about 3% which is substantially smaller than the size of the dip. Continued operation of IceCube in future will reduce this error further. Large errors are due to systematics: mostly due to uncertainties in the total normalization and tilt of the spectrum. To a large extent they can be eliminated when searching for the dip. Indeed, the systematics has smooth dependence on energy, the systematic errors in different bins are strongly correlate. One can parametrize these uncertainties by a few parameters and determine them by fitting data.

The problem of smearing does not exist in the case of the zenith angle distribution, since muons nearly follow neutrinos, and the zenith angle resolution is $0.5 - 1^\circ$. We compute the number of events N_j in a given zenith angle bin $\Delta_j \cos \theta_z$ using (22) and performing integration from the threshold E_{th} :

$$N_j = 2\pi \int_{\Delta_j \cos \theta_z} d \cos \theta_z \int_{E_{th}} dE \Phi_\nu^0(E, \theta_z) A_{\text{eff}}(E, \theta_z) P_{\mu\mu}(E, \theta_z) + \text{antineutrinos}. \quad (23)$$

We then define the suppression factors in the individual bins as

$$S_j = \frac{N_j}{N_j^0}, \quad (24)$$

where N_j^0 are the numbers of events without oscillations which correspond to $P_{\mu\mu} = 1$ in (23). In Figs. 6 and 7 we show the zenith angle dependence of the suppression factor for different values of the mixing parameter $\sin^2 \alpha$ and $\sin^2 \theta_{23} = 1/2$ (this corresponds to $|U_{\mu 0}|^2 = 0.5 \sin^2 \alpha$) and two different thresholds $E_{th} = 100$ GeV (Fig. 6) and $E_{th} = 1$ TeV (Fig. 7). Oscillations lead to distortion of the zenith angle distribution. For nearly horizontal direction the effect is mainly due to vacuum oscillations which have enough baseline to develop if $E \lesssim 0.5$ TeV. In this case the averaged oscillation effect is given by $1 - 2|U_{\mu 0}|^2(1 - |U_{\mu 0}|^2) \approx 1 - \sin^2 \alpha$ in agreement with the results of Figs. 6 and 7. The matter effect increases with $|\cos \theta_z|$. According to these figures substantial differences between the energy-integrated distribution with and without sterile mixing are expected

in the bins near the vertical direction. For $\sin^2 \alpha = 0.04$ the effect is about 20% and the statistical errors, 3%, are much smaller. For other mixing schemes the distortion can be different. In particular, in the ν_s -flavor mixing scheme maximal suppression is in the bins $\cos \theta_z = (-0.9, -0.8)$ (see Sec. 5).

For vertical directions the evaluation of the suppression (integrated over the energy) can be done using the survival probabilities of Figs. 1 and 2. If *e.g.* $\sin^2 \alpha = 0.08$, the probabilities averaged over the median energy interval in the neutrino and antineutrino channels are $P_{\mu\mu} = 0.6$ and $\bar{P}_{\mu\mu} = 0.8$ respectively. Then averaging the contributions of the neutrinos and antineutrinos we obtain $S \sim \langle P \rangle = 0.70 - 0.75$, in agreement with results in Figs. 6 and 7. With increase of threshold, the effect of vacuum oscillations in nearly horizontal directions becomes smaller. The effect in the $\bar{\nu}$ channel increases, whereas in the ν channel it decreases, thus compensating the overall change.

In Fig. 8 we confront the experimental results with the predicted zenith angle distributions computed as

$$N_j = N_j^{MC} S_j,$$

where N_j^{MC} is taken according to the IceCube simulation (see Fig. 19 from [13]). We have implemented an overall normalization and tilt of the distribution, as we discuss below in (25).

4 Bounds on parameters of sterile neutrinos

To get an idea of the sensitivity of the currently available IceCube data to the sterile neutrino mixing we have performed a χ^2 fit of the IceCube zenith angle distribution. For a given “model” of mixing characterized by $(\Delta m_{03}^2, \sin^2 \alpha)$ we compute the expected number of muon events N_j^{mod} in the zenith angle bin j . For this we use the IceCube simulation, N_j^{MC} [13]:

$$N_j^{\text{mod}}(C, \tau; \Delta m_{03}^2, \sin \alpha) = C[1 + \tau(\cos \theta_j + 0.5)]N_j^{MC} S_j(\Delta m_{03}^2, \sin^2 \alpha), \quad (25)$$

where C is an overall normalization parameter and τ is a zenith angle tilt parameter. The model without ν_s mixing is recovered when $\alpha = 0$. We compare the expected numbers N_j^{mod} with data N_j^{dat} and the χ^2 is defined as

$$\chi^2(C, \tau; \Delta m_{03}^2, \sin \alpha) = \sum_j \frac{\left(N_j^{\text{dat}} - N_j^{\text{mod}}(C, \tau; \Delta m_{03}^2, \sin \alpha)\right)^2}{\left(\sigma_j^{\text{dat}}\right)^2}. \quad (26)$$

The variance σ_j^{dat} is calculated by adding in quadrature the statistical and systematic uncertainties as given by IceCube [13]. For our analysis we use the IceCube data in the range of zenith angles $-1 \leq \cos \theta_z \leq -0.1$ (*i.e.*, bins $j = 1-18$), leaving out the last two near horizontal bins where the detector response is not well-understood and contamination of the

atmospheric muons is possible. For fixed values $(\Delta m_{03}^2, \sin^2 \alpha)$ we minimize the χ^2 varying the (C, τ) parameters. The difference

$$\Delta\chi^2 = \chi_{\min}^2(C, \tau; \Delta m_{03}^2, \sin^2 \alpha) - \chi_{\min}^2(C, \tau; \Delta m_{03}^2, 0)$$

quantifies the rejection significance of the ν_s mixing model with respect to the model without ν_s mixing.

In Table 1 we show results of our statistical analysis which is reduced to determination of the minimal χ^2 values of C and τ for given Δm_{03}^2 and $\sin^2 \alpha$. We show χ_{\min}^2 and the best fit values of C and τ for the case of statistical errors for the individual bins only. Also shown is the fit for the “null” hypothesis. Notice that the ν_s mixing $\sin^2 \alpha \sim 0.01$ fits the data better than the model without ν_s mixing (“null” model) $\Delta\chi^2 < 0$. Also notice that for $\sin^2 \alpha \lesssim 0.04$, C and τ are below 3% and then they quickly increase with α reaching 12 – 13% for $\sin^2 \alpha = 0.08$.

Table 1: Results of the χ^2 –analysis of the IceCube zenith angle distribution. Shown are χ_{\min}^2 as well as the best fit values of the normalization parameter C and tilt τ for given values of Δm_{03}^2 and $\sin^2 \alpha$.

Δm_{03}^2 (eV ²)	$\sin^2 \alpha$	χ_{\min}^2	C	τ
0.5	0.005	14.09	0.991	0.0175
	0.01	15.29	0.997	0.0086
	0.02	16.50	1.008	-0.0082
	0.04	18.88	1.032	-0.0394
	0.08	31.73	1.085	-0.1238
1.0	0.005	14.56	0.991	0.0217
	0.01	15.33	0.997	0.0126
	0.02	16.97	1.010	-0.0052
	0.04	20.19	1.033	-0.0347
	0.08	39.41	1.092	-0.1344
2.0	0.005	14.40	0.991	0.0247
	0.01	14.45	0.996	0.0184
	0.02	16.11	1.008	0.0043
	0.04	21.87	1.034	-0.0323
	0.08	43.29	1.094	-0.1298
3.0	0.005	14.03	0.991	0.0246
	0.01	14.92	0.996	0.0166
	0.02	15.84	1.008	0.0079
	0.04	18.66	1.033	-0.0217
	0.08	41.98	1.098	-0.1387
IceCube	sim.	14.16	0.982	0.04024

Fig. 9 (left panel) shows the bounds on the sterile neutrino mixing as function of Δm_{03}^2 from the analysis which takes into account statistical uncertainty in each bin as well as the

systematic uncertainties due to overall normalization and tilt of the zenith angle distribution. These are the main uncertainties. To illustrate possible effect of other systematics we have taken the extreme case: 5% uncorrelated errors for individual bins (see Fig. 9, right panel). (Although it is expected that other possible uncertainties are smooth functions of the zenith angle and therefore correlate in different bins.) In reality the effect of additional errors should be smaller than that. The parameter space to the right hand side from the lines in Fig. 9 is excluded at the indicated confidence level.

The bounds weakly depend on the Δm_{03}^2 , as can be seen from the behavior of the suppression factors (Figs. 6 and 7). The bounds are slightly weaker for smaller Δm_{03}^2 since in this case the resonance dip shifts from the energy range where IceCube has the highest sensitivity.

We find that with statistical uncertainties only (left panel) the upper bound is $\sin^2 \alpha < 0.05$ or $|U_{\mu 0}|^2 < 0.025$ at 3σ level and $\Delta m_{03}^2 = 1 \text{ eV}^2$. At 2σ level the bounds are $\sin^2 \alpha < 0.04$ and $|U_{\mu 0}|^2 < 0.02$. At the same time interpretation of the LSND/MiniBooNE results in terms of oscillations in the presence of sterile neutrinos requires $|U_{\mu 0}|^2 \gtrsim 0.03$ for $\Delta m_{03}^2 = 1 \text{ eV}^2$, and $|U_{\mu 0}|^2 \gtrsim 0.06$ for $\Delta m_{03}^2 = 0.5 \text{ eV}^2$.

With 5% uncorrelated systematic errors (Fig. 9 right panel) the limits become substantially weaker: $\sin^2 \alpha = 0.06$, is excluded at 90% C.L. only.

5 The ν_s –flavor mixing in the leading approximation

Let us consider dependence of effects of the ν_s –oscillations on the mixing scheme. In the leading order approximation, which is valid at high energies ($E > 0.5 \text{ TeV}$), the results can be immediately obtained from our consideration in Sec. 2. A detailed analysis of the observables in IceCube and bound on parameters of the ν_s –flavor mixing will be given elsewhere [19].

Let us consider first the $\nu_s - \nu_\mu$ mixing only, *i.e.*, the simplest scheme of ν_s –flavor mixing. The corresponding mixing matrix in the flavor basis $(\nu_s, \nu_\tau, \nu_\mu)$ equals

$$U_f = U_{24}U_{23} = \begin{pmatrix} c_{24} & -s_{24}s_{23} & s_{24}c_{23} \\ 0 & c_{23} & s_{23} \\ -s_{24} & -c_{24}s_{23} & c_{24}c_{23} \end{pmatrix}, \quad (27)$$

where $s_{24} \equiv \sin \theta_{24}$, *etc.*. Formally it differs from the mixing in (1) by permutation of U_{23} with the ν_s –mixing matrix.

Now the mixing matrix elements, which determine the oscillations with splitting Δm_{03}^2 , equal $U_{s0} = c_{24}$, $U_{\tau 0} = 0$, $U_{\mu 0} = -s_{24}$. They are reduced to the elements of our simplest case (5), if formally we take $c_{23} = 0$ and $s_{23} = -1$ and $\alpha = \theta_{24}$. Therefore in the leading order approximation for high energies the probabilities can be obtained from the probabilities in

ν_s -mass mixing case by taking $s_{23} = -1$. In particular, according to (14)

$$P_{\mu\mu}^{(f)} \equiv |A_{\mu\mu}|^2 \approx |A_{\tau'\tau'}(\theta_{24})|^2. \quad (28)$$

For $A_{\tau'\tau'} = -1$ we obtain $P_{\mu\mu}^f = 1$, whereas in the ν_s -mass mixing scheme this value gives the minimum of the dip $P_{\mu\mu}^{(mass)} = 0$.

It is possible to find relation between the sizes of dips for different mixing schemes. For maximal 2-3 mixing we have from (14) the survival probability in the ν_s -mass mixing scheme (2):

$$P_{\mu\mu}^{(mass)} = \frac{1}{4} |A_{\tau'\tau'} + 1|^2. \quad (29)$$

In the resonance, the amplitude $A_{\tau'\tau'}$ is approximately real. This can be seen using explicit results for the constant density case. Indeed, according to (48) in resonance $H_{1m} = -H_{2m}$, and therefore (49) gives $A_{\tau'\tau'} \approx \cos(H_{1m}x)$. Then from (29) and (28) we obtain relation between the probabilities:

$$P_{\mu\mu}^{(f)} = \left(2\sqrt{P_{\mu\mu}^{(mass)}} - 1 \right)^2. \quad (30)$$

Our numerical results in Fig. 10 confirm this relation.

Let us consider corrections to the leading order result due to oscillations driven by the 2-3 mixing and splitting. They are sub-dominant at high energies, but become dominant at low energies. In the ν_s -flavor mixing case it is convenient to consider oscillations immediately in the flavor basis, *i.e.* take the flavor basis as the propagation one. Using the mixing matrix (27) we find the Hamiltonian of evolution $H = U_f H^{diag} U_f^T + V$ which can be represented in the following form

$$H = \frac{\Delta m_{03}^2}{2E} \begin{pmatrix} c_{24}^2 - \frac{2EV_\mu}{\Delta m_{03}^2} & 0 & -s_{24}c_{24} \\ 0 & 0 & 0 \\ -s_{24}c_{24} & 0 & s_{24}^2 \end{pmatrix} - \frac{\Delta m_{32}^2}{2E} \begin{pmatrix} s_{24}^2 c_{23}^2 & s_{24}s_{23}c_{23} & s_{24}c_{24}c_{23}^2 \\ s_{24}s_{23}c_{23} & s_{23}^2 & c_{24}s_{23}c_{23} \\ s_{24}c_{24}c_{23}^2 & c_{24}s_{23}c_{23} & c_{24}^2 c_{23}^2 \end{pmatrix}. \quad (31)$$

At high energies the evolution is described by the first term of the Hamiltonian (which does not depend on the 2-3 mixing), ν_τ decouples and the corresponding S matrix in the flavor basis can be written as

$$S = \begin{pmatrix} A_{ss} & 0 & A_{s\mu} \\ 0 & 1 & 0 \\ A_{\mu s} & 0 & A_{\mu\mu} \end{pmatrix}. \quad (32)$$

So that the survival probability, $P_{\mu\mu} = |A_{\mu\mu}|^2$, is in accordance with (28). Indeed, the first term of the Hamiltonian (31) coincides with the Hamiltonian (8) up to permutation of the 2-3 lines, 2-3 columns and substitution $\alpha \rightarrow \theta_{24}$, and therefore $A_{\mu\mu} = A_{\tau'\tau'}$ in this approximation. With the sub-leading term of the Hamiltonian taken into account, evolution is not reduced to the 2ν -evolution.

In Fig. 10 (upper panel) we show the probabilities for the ν_s -flavor mixing scheme. According to this figure the dip for $\cos\theta_z = -1$ is suppressed and maximal suppression is

achieved at $\cos\theta_z = -0.90$, in contrast to the mass-mixing case. Also here the size of the dip decreases slower with increase of $\cos\theta_z$. This result holds for other mixing angles: if $\sin^2\theta_{24} = 0.08$, in the vertical bin we have $P_{\mu\mu}^{(f)}(\cos\theta_z = -1) \approx 1$, and maximal suppression in the dip, $P_{\mu\mu}^{(f)} = 0$, is achieved at $\cos\theta_z = -0.80$. Thus, the zenith angle distributions are different for the ν_s -flavor and mass mixing schemes. Furthermore, in the dip region ν_μ is transformed mainly to ν_s . So, the appearance of ν_τ is the signature of the ν_s -mass mixing scheme.

The low energy ($E < 0.5$ TeV) behavior of probabilities is also different in these mixing cases. Indeed, in the basis ν_a defined in such a way that $\nu_f = U_{24}\nu_a$ the Hamiltonian is given by

$$H_a = U_{23}H^{diag}U_{23}^T + U_{24}^T V U_{24} ,$$

or explicitly

$$H_a = \begin{pmatrix} \frac{\Delta m_{03}^2}{2E} - c_{24}^2 V_\mu & 0 & -s_{24}c_{24}V_\mu \\ 0 & -s_{23}^2 \frac{\Delta m_{32}^2}{2E} & -s_{23}c_{23} \frac{\Delta m_{32}^2}{2E} \\ \dots & \dots & -c_{23}^2 \frac{\Delta m_{32}^2}{2E} - s_{24}^2 V_\mu \end{pmatrix}. \quad (33)$$

For energies much below the sterile resonance, $V_\mu \ll \frac{\Delta m_{03}^2}{2E}$, one can perform a block diagonalization thus decoupling the heaviest state, or simply neglect the 1-3 terms $s_{24}c_{24}V_\mu$ in the Hamiltonian (33). The latter is equivalent to an approximation of negligible matter effect on the angle θ_{24} . So, the evolution is reduced to 2ν - problem. Similarly to our consideration in Sec. 2 we find (returning to the flavor basis) that the $\nu_\mu - \nu_\mu$ survival probability equals

$$P_{\mu\mu} \approx |c_{24}^2 A_{\mu\mu}^{(a)} + s_{24}^2 A_{ss}^{(a)}|^2, \quad (34)$$

where $A_{ss}^{(a)} = \exp[-ix(\frac{\Delta m_{03}^2}{2E} - c_{24}^2 V_\mu)]$, and the amplitude $A_{\mu\mu}^{(a)}$ should be obtained by solving the evolution equation with the Hamiltonian

$$H_a^{(2)} \approx - \begin{pmatrix} 0 & \sin 2\theta_{23} \frac{\Delta m_{32}^2}{4E} \\ \sin 2\theta_{23} \frac{\Delta m_{32}^2}{4E} & \cos 2\theta_{23} \frac{\Delta m_{32}^2}{2E} + s_{24}^2 V_\mu \end{pmatrix}. \quad (35)$$

Here we have subtracted from the 2×2 submatrix of (33) the matrix proportional to the unit matrix. The $\nu_\mu - \nu_\mu$ probability averaged over fast oscillations driven by Δm_{03}^2 equals

$$P_{\mu\mu} = c_{24}^4 |A_{\mu\mu}^{(a)}|^2 + s_{24}^4 \approx c_{24}^4 |A_{\mu\mu}^{(a)}|^2. \quad (36)$$

The matter effect on the amplitude $A_{\mu\mu}^{(a)}$ becomes substantial when

$$\frac{\Delta m_{32}^2}{4E} \sim s_{24}^2 |V_\mu|,$$

i.e., $E \sim 150(0.04/s_{24}^2)$ GeV. Matter suppresses the depth of $\nu_\mu - \nu_\tau$ oscillations and increases the phase velocity as compared to the vacuum oscillation case. For the maximal 2-3 mixing the effect is the same in the neutrino and antineutrino channels:

$$\phi_{32} = x \sqrt{(\Delta m_{32}^2/2E)^2 + (s_{24}^2 V_\mu)^2}.$$

For non-maximal 2-3 mixing the resonance is realized at

$$E = -\frac{\Delta m_{32}^2}{2s_{24}^2 V_\mu} \cos 2\theta_{23},$$

and picture becomes $\nu - \bar{\nu}$ asymmetric depending on $\cos 2\theta_{23}$. We find that for $\theta_{23} = \pi/4$, $s_{24}^2 = 0.04$ and $\cos \theta_z = -1.0$ the averaged (over fast oscillations) corrections to the probabilities in both channels equal $\Delta P_{\mu\mu} \approx 0.15$ at $E = 100$ GeV and $\Delta P_{\mu\mu} \approx 0.02$ at $E = 300$ GeV.

Let us consider the generic ν_s -flavor mixing. The mixing matrix can be written as $U_f = U_{34}U_{24}U_{23}$, where U_{34} is the matrix of rotation in the $\nu_s - \nu_\tau$ plane on the angle θ_{34} . The matrix elements which describe the flavor content of ν_0 equal

$$U_{s0} = c_{34}c_{24}, \quad U_{\tau 0} = -s_{34}c_{24}, \quad U_{\mu 0} = -s_{24}. \quad (37)$$

The ν_μ oscillations in vacuum (LSND/MiniBooNE) are determined by the parameter $U_{\mu 0}$ – the admixture of the muon neutrino in the heaviest state. In matter at high energies the phase ϕ_{32} is small and can be neglected, then the relevant parameters are $U_{\mu 0}$, $U_{\tau 0}$, U_{s0} . The Hamiltonian can be written as

$$H = \frac{\Delta m_{03}^2}{2E} V_0 \times V_0^T + V + O\left(\frac{\Delta m_{03}^2}{2E}\right),$$

where $V_0^T \equiv (U_{s0}, U_{\tau 0}, U_{\mu 0})$.

Comparing (37) with the elements in (5) we conclude that the dominant oscillation results at high energies in the flavor case can be obtained from the results in the ν_s -mass mixing scheme identifying

$$c_{34}c_{24} = c_\alpha, \quad s_{24} = -s_\alpha s_{23}, \quad s_{34}c_{24} = s_\alpha c_{23}.$$

That is, in general according to (14) the probability equals

$$P_{\mu\mu} \approx \left| \sin^2 \beta A_{\tau'\tau'}(\alpha) + \cos^2 \beta \right|^2, \quad (38)$$

where $c_\alpha = c_{34}c_{24}$ or

$$s_\alpha^2 = s_{24}^2 + s_{34}^2 - s_{34}^2 s_{24}^2 \approx s_{34}^2 + s_{24}^2, \quad (39)$$

and

$$\sin^2 \theta_{23} = \frac{s_{24}^2}{s_{24}^2 + s_{34}^2 - s_{34}^2 s_{24}^2} \approx \frac{s_{24}^2}{s_{24}^2 + s_{34}^2}. \quad (40)$$

Explicitly,

$$P_{\mu\mu} \approx \frac{1}{(1 - c_{24}^2 c_{34}^2)^2} \left| s_{24}^2 A_{\tau'\tau'} + s_{34}^2 c_{24}^2 \right|^2. \quad (41)$$

In Fig. 10 (middle and bottom panels) we show the survival probabilities as functions of energy for fixed value $s_{24}^2 = 0.04$ (as is required by LSND/MiniBooNE) and different values of $\sin^2 \beta$. Notice that for the core crossing trajectories with change of mixing scheme the size and form of the oscillation dip changes significantly. The ν_s -mass mixing case corresponds to $\sin^2 \beta = 0.5$ or $s_{24}^2 \approx s_{34}^2$, whereas the $\nu_s - \nu_\mu$ mixing case is realized when $\sin^2 \beta = 1$, that is $s_{34}^2 = 0$. Recall that at low energies the sub-leading effects due to Δm_{32}^2 become important.

In Fig. 11 we show the zenith angle dependence of the suppression factor integrated over the energy (see definition in (24)) for $s_{24}^2 = 0.04$ and different values of $\sin^2 \beta$. Starting from $\sin^2 \beta = 1$ ($s_{34}^2 = 0$) and reducing it down to 0.08 one obtains first flat distribution, then the distribution with a dip at or near the vertical directions and then again rather flat distribution. In all the cases the suppression weakens in the bins close to horizon.

The dip is at $|\cos \theta_z| \gtrsim 0.8$ in Fig. 11. Indeed, in the $\nu_s - \nu_\mu$ mixing case maximal suppression $P_{\mu\mu} = 0$ corresponds to $A_{\tau'\tau'} = 0$. For the mantle-crossing trajectories ($|\cos \theta_z| \lesssim 0.8$) this can be achieved if the MSW resonance condition and the oscillation phase condition $\phi_{03} = \pi$ are satisfied simultaneously (see also discussion in [11]). The conditions can be rewritten as

$$\frac{2\pi}{l_\nu} \cos 2\theta_{24} = V_\mu, \quad 2x = \frac{l_\nu}{\sin 2\theta_{24}},$$

where l_ν is the oscillation length in vacuum, $x = 2R_E |\cos \theta_z|$ is the length of neutrino trajectory (R_E is the radius of the Earth), and the expression in the RHS of the second equality gives the oscillation length in resonance. From these conditions, excluding l_ν , we find

$$|\cos \theta_z| = \frac{\pi}{2R_E V_\mu \tan 2\theta_{24}}. \quad (42)$$

Thus, a shift of the dip to small $|\cos \theta_z|$ would require large $\nu_s - \nu_\mu$ mixing angle θ_{24} . The latter is restricted by MINOS experiment [20]: $\sin^2 2\theta_{24} < 0.14$ (90% C.L.), and for the allowed values of θ_{24} the condition (42) can not be satisfied (see also [21]). Large mixing α in the 2ν amplitude $A_{\tau'\tau'}$ is possible if s_{34}^2 is large. However, in this case also $\sin^2 \beta$ is substantially below 1. According to (38), $P_{\mu\mu} = 0$ corresponds to $A_{\tau'\tau'}(\alpha) = -\cot^2 \beta$, *i.e.* negative amplitude. In turn, this requires even bigger phase than in the previous case, $\phi_{03} > \pi$, which can not be achieved.

Notice that for values of oscillation parameters

$$\Delta m_{03}^2 \sim (0.5 - 1) \text{ eV}^2, \quad \sin^2 \alpha \sim 0.04, \quad \sin^2 \beta \sim 1, \quad (43)$$

the zenith angle distribution (suppression factor) for $|\cos \theta_z| > 0.1$ is rather flat in spite of profound and wide dips in the oscillation probabilities. A shallow dip in the suppression factor can appear in the interval of $\cos \theta_z$ ($-0.95, -0.8$) for $\Delta m_{03}^2 \sim 0.5 \text{ eV}^2$. For $|\cos \theta_z| < 0.1$ the suppression becomes weaker which one can still use to disentangle the oscillation effect and normalization of spectrum. This flatness of the energy integrated distribution is

due to (i) specific dependence of the IceCube sensitivity on energy and (ii) correlated change of properties of the oscillation dip with change of θ_z which is realized for the parameters (43). According to Fig. 10 (upper panel) with increase of $\cos\theta_z$ the dip shifts to higher energies, its depths first increases and then decreases, and the width becomes wider.

The zenith angle distribution with parameters (43) could give even better fit, with a decrease in χ_{\min}^2 value by 3, of the observed distribution than the null oscillation hypothesis. Furthermore the required values of the overall normalization, 1.057, and tilt, 0.0136, are small. The contribution from low energy oscillations driven by 2-3 mixing and mass splitting, however, has strong dependence on the zenith angle, and consequently, distorts the distribution near vertical directions. Apparently study of the zenith angle distributions with different energy thresholds or in different energy intervals will enhance sensitivity to oscillation effects.

Thus, apart from special case of ν_s -flavor mixing in the leading order approximation, the allowed mixing schemes predict the dip in the zenith angle distribution in the vertical or nearly vertical directions, and therefore are disfavored by the present IceCube data, as in the illustrative analysis in Sec. 4.

Let us compare our results with those in Refs. [10] and [11]. In [10] the flavor mixing has been considered with $s_{24}^2 = 0.045$ and $s_{34}^2 = 0.45$ (*i.e.*, with nearly maximal $\nu_s - \nu_\tau$ mixing). According to (40) these parameters correspond to $\sin^2\beta = 0.095$, and consequently, $P_{\mu\mu} \approx |0.095A_{\tau'\tau'} + 0.905|^2$. This leads to $\sim 10 - 20\%$ effect with weak dependence on the zenith angle and energy (see Fig. 4 in [10]). Furthermore, since $s_\alpha^2 \approx 0.5$ (see (39)), the mixing is nearly maximal and therefore the resonance dip is absent (see Fig. 3e in [10]). In [11] the ν_s -flavor mixing is considered with $s_{24}^2 = s_{34}^2 = 0.04$. This equality means that in fact the ν_s -mass mixing is realized with $s_\alpha^2 \approx 2s_{24}^2 = 0.08$. Our results are in agreement with those in Fig. 5a of [11]. Our interpretation of the dip at $\cos\theta_z = -1$, however, differs: the dip is due to parametric enhancement of oscillations, rather than the MSW oscillation dip in the medium with averaged density.

Thus, the zenith angle and the energy distributions of events substantially depend on details of the mixing scheme, and in particular on mixing of ν_τ in ν_0 determined by s_{34} .

6 Conclusions

1. We have considered the neutrino oscillations in the Earth in the presence of single sterile neutrino with mass $m \sim 1$ eV [$\Delta m_{03}^2 = (0.5 - 3)$ eV²].

2. We present an analytic study of the oscillation probabilities which allows one to understand features of dependences of the probabilities on various parameters, and in particular, on the mixing scheme. We have identified the simplest mixing scheme in which the flavor evolution is reduced to the 2ν evolution. We showed how results for other mixing schemes can be obtained from the results of the simplest scheme.

3. The main features of probabilities (in the ν_s -mass mixing scheme) include the resonance dips (peaks) in the $\bar{\nu}$ -channel in the energy range (0.5 – 5) TeV: the MSW resonance peak for the mantle crossing trajectories and the parametric enhancement peak for the core crossing trajectories. In the ν -channel at $E < 0.5$ TeV there is the matter enhanced $\mu - \tau$ transition due to oscillations induced by the 2-3 mixing and mass splitting. The phase velocity in the neutrino channel is enhanced due to matter effect, so that oscillations are developed already for $E = (0.1 - 0.5)$ TeV. In contrast, in the antineutrino channel, matter suppresses the phase velocity and oscillations are not developed. These features can be modified in other mixing schemes.

4. Oscillation effects on the ν_μ - and $\bar{\nu}_\mu$ - atmospheric neutrino fluxes and on the sum of the fluxes are studied. We have computed the energy spectra of these neutrinos, integrated over various zenith angle intervals. Maximal oscillation effect is $\sim 40\%$ suppression of the flux in a wide (half an order of magnitude) energy interval. The position of the dip is determined by the value of Δm_{03}^2 . The dip has low energy tail due to oscillations driven by the 2-3 mixing. In the range (0.5 - 5) TeV the effect is mainly due the resonance dip in the $\bar{\nu}$ -channel, whereas in the range (0.1 - 0.5) TeV it is mainly due to $\nu_\mu - \nu_\tau$ oscillations with matter modified frequency in the ν -channel. Changes of the energy threshold does not modify results substantially.

5. We have computed the zenith angle distributions of muon events (induced by ν_μ and $\bar{\nu}_\mu$) in the IceCube detector. Oscillations lead to typical distortion of this distribution with about $(1 - \sin^2 \alpha)$ suppression in the directions close to the horizon, and stronger suppression in the directions close to vertical $|\cos \theta_z| > 0.7$. For the ν_s -mass mixing scheme, the maximal suppression, 20 – 25%, is in the vertical direction.

6. The relative oscillation effect on the energy spectrum of neutrinos can be enhanced by making integration over directions near the vertical one.

7. We confronted the computed distributions with the IceCube data and performed χ^2 fit of the zenith angle distribution for the ν_s -mass mixing. We find that with statistical errors and systematic uncertainties in the total normalization and tilt the values, $|U_{\mu 0}|^2 > 0.025$ are excluded at more than 3σ level. The central value required by LSND/MiniBooNE is $|U_{\mu 0}|^2 \sim 0.03$ is excluded at the 3σ level. With additional 5% uncorrelated systematic uncertainties the limits become much weaker.

8. We have studied the oscillation effects in generic ν_s -flavor mixing scheme in the leading order approximations valid for high energies $E \gtrsim 0.5$ TeV. We find that maximal suppression is in the bins $\cos \theta_z = (-1.0, -0.8)$. Rather flat zenith angle distribution can be obtained in pure $\nu_\mu - \nu_s$ mixing case with $|U_{\mu 0}|^2 \sim 0.04$ and $\Delta m_{03}^2 \sim 0.5 \text{ eV}^2$ as well as for large $\nu_\tau - \nu_s$ mixing: $|U_{\tau 0}|^2 \sim 0.5$. Fit to the zenith angle event distribution substantially improves for this case and gives a better description of data than the no ν_s - mixing case. Future studies of the zenith angle distributions with different energy thresholds or in different energy intervals will allow to perform very sensitive search for sterile neutrinos.

Acknowledgments

We thank Doug Cowen, Kara Hoffman, Paolo Desiati, Elisa Resconi and specially Warren Huelsnitz for helping us understand the IceCube results better. Work of S.R. was performed at and under the sponsorship of the U.S. Naval Research Laboratory.

Appendix. Constant density case

To a good approximation the case of constant density can be applied for neutrinos crossing the mantle of the Earth only. For constant V_μ the Hamiltonian (8) can be diagonalized by the rotation on the mixing angle in matter α_m :

$$\sin^2 2\alpha_m = \frac{\sin^2 2\alpha}{\left(\cos 2\alpha - \frac{2V_\mu E}{\Delta m_{03}^2}\right)^2 + \sin^2 2\alpha}. \quad (44)$$

Integration of the evolution equation is then trivial, giving the S -matrix

$$S_m = \begin{pmatrix} e^{-iH_{1m}x} & 0 & 0 \\ 0 & e^{-iH_{2m}x} & 0 \\ 0 & 0 & e^{i\phi_{32}} \end{pmatrix}, \quad (45)$$

where H_{im} are the eigenvalues of the Hamiltonian in matter:

$$H_{1m,2m} = \frac{1}{2} \left(\frac{\Delta m_{03}^2}{2E} - V_\mu \right) \pm \frac{\Delta m_{03}^2}{4E} \sqrt{\left(\cos 2\alpha - \frac{2EV_\mu}{\Delta m_{03}^2} \right)^2 + \sin^2 2\alpha}. \quad (46)$$

H_{1m} corresponds to the + sign. In the antineutrino (resonance) channel the eigenvalues, as functions of neutrino energy, have the following asymptotics:

$$H_{1m} \approx \begin{cases} \frac{\Delta m_{03}^2}{2E} - V_\mu \cos^2 \alpha, & E \rightarrow 0; \\ \frac{\Delta m_{03}^2}{4E} \sin 2\alpha, & \text{resonance}; \\ \frac{\Delta m_{03}^2}{2E} \sin^2 \alpha, & \frac{\Delta m_{03}^2}{2E} \ll V_\mu. \end{cases} \quad (47)$$

$$H_{2m} \approx \begin{cases} -V_\mu \sin^2 \alpha, & E \rightarrow 0; \\ -\frac{\Delta m_{03}^2}{4E} \sin 2\alpha, & \text{resonance}; \\ -V_\mu, & \frac{\Delta m_{03}^2}{2E} \ll V_\mu. \end{cases} \quad (48)$$

Since for antineutrinos $V_\mu > 0$, one has $H_{2m} < 0$. In the limit of high energies: $H_{1m} - H_{2m} = V_\mu$.

Returning back to the $\tilde{\nu}$ basis, $\tilde{S} = U(\alpha_m)S_mU^\dagger(\alpha_m)$, we obtain

$$A_{\tau'\tau'} = \sin^2 \alpha_m e^{-iH_{1m}x} + \cos^2 \alpha_m e^{-iH_{2m}x}. \quad (49)$$

Then insertion of this amplitude in (14) gives

$$P_{\mu\mu} = \left| \sin^2 \theta_{23} \left(\sin^2 \alpha_m e^{-iH_{1m}x} + \cos^2 \alpha_m e^{-iH_{2m}x} \right) + \cos^2 \theta_{23} e^{i\phi_{32}} \right|^2, \quad (50)$$

and explicitly:

$$P_{\mu\mu} = 1 - \sin^4 \theta_{23} \sin^2 2\alpha_m \sin^2(\phi_1 - \phi_2) - \sin^2 2\theta_{23} (\sin^2 \alpha_m \sin^2 \phi_1 + \cos^2 \alpha_m \sin^2 \phi_2). \quad (51)$$

Here

$$\begin{aligned} \phi_1 &= \frac{1}{2}(H_{1m}x + \phi_{32}) = \frac{1}{2} \left(H_{1m} + \frac{\Delta m_{32}^2}{2E} \right) x, \\ \phi_2 &= \frac{1}{2}(H_{2m}x + \phi_{32}) = \frac{1}{2} \left(H_{2m} + \frac{\Delta m_{32}^2}{2E} \right) x, \end{aligned} \quad (52)$$

and consequently,

$$\phi_1 - \phi_2 = \frac{1}{2}(H_{1m} - H_{2m})x. \quad (53)$$

If $E \rightarrow 0$ (vacuum oscillation limit), $H_{2m} \rightarrow 0$ and $H_{1m} \rightarrow \frac{\Delta m_{03}^2}{2E}$. Therefore

$$\phi_1 \rightarrow \frac{\Delta m_{02}^2}{4E}x, \quad \phi_2 \rightarrow \frac{\Delta m_{32}^2}{4E}x, \quad \phi_1 - \phi_2 = \frac{\Delta m_{03}^2}{4E}x. \quad (54)$$

In this case also $\alpha_m \rightarrow \alpha$ and the averaged over fast oscillations probability equals

$$\bar{P}_{\mu\mu} = 1 - \cos^2 \alpha \sin^2 2\theta_{23} \sin^2 \frac{\Delta m_{32}^2 x}{4E} - 0.5 \sin^4 \theta_{23} \sin^2 2\alpha - 0.5 \sin^2 2\theta_{23} \sin^2 \alpha. \quad (55)$$

The first two terms correspond (up to $\cos^2 \alpha$) to the standard 2-3 probability and corrections are of the order $\sin^2 \alpha$.

In the limit of high energies for antineutrinos we have $H_{1m} \rightarrow \frac{\Delta m_{03}^2}{2E} \sin^2 \alpha$ and $H_{2m} \rightarrow -|V_\mu|$. So,

$$\phi_1 = \frac{1}{2} \left(\frac{\Delta m_{03}^2}{2E} \sin^2 \alpha + \frac{\Delta m_{32}^2}{2E} \right) x \approx \frac{\Delta m_{03}^2 x}{4E} \sin^2 \alpha, \quad (56)$$

$$\phi_2 = \frac{1}{2}(-|V_\mu|x + \phi_{32}) \approx -\frac{1}{2}|V_\mu|x. \quad (57)$$

For high energies (above the resonance): $\alpha_m \approx 90^\circ$, and consequently,

$$P_{\mu\mu} \approx 1 - \sin^2 2\theta_{23} \sin^2 \phi_1 \approx 1 - \sin^2 2\theta_{23} \sin^2 \left(\frac{\Delta m_{03}^2 x}{4E} \sin^2 \alpha \right). \quad (58)$$

In the case of constant density the $\nu'_\tau - \nu'_\tau$ probability is described by usual oscillation formula:

$$P_{\tau'\tau'} = 1 - \sin^2 2\alpha_m \sin^2 \phi_m, \quad (59)$$

where ϕ_m is the half-phase of oscillations in matter:

$$\phi_m = \frac{\Delta m_{03}^2 x}{4E} \sqrt{\left(\cos 2\alpha - \frac{2V_\mu E}{\Delta m_{03}^2} \right)^2 + \sin^2 2\alpha}. \quad (60)$$

References

- [1] A. Aguilar *et al.* [LSND Collaboration], Phys. Rev. **D64** (2001) 112007. [hep-ex/0104049].
- [2] A. A. Aguilar-Arevalo *et al.* [The MiniBooNE Collaboration], Phys. Rev. Lett. **105** (2010) 181801, [arXiv:1007.1150 [hep-ex]].
- [3] G. Mention, M. Fechner, T. Lasserre, T. A. Mueller, D. Lhuillier, M. Cribier, A. Letourneau, [arXiv:1101.2755 [hep-ex]].
T. A. Mueller, D. Lhuillier, M. Fallot, A. Letourneau, S. Cormon, M. Fechner, L. Giot, T. Lasserre *et al.*, [arXiv:1101.2663 [hep-ex]].
- [4] J. N. Abdurashitov, V. N. Gavrin, S. V. Girin, V. V. Gorbachev, P. P. Gurkina, T. V. Ibragimova, A. V. Kalikhov, N. G. Khairnasov *et al.*, Phys. Rev. **C73** (2006) 045805. [nucl-ex/0512041].
J. N. Abdurashitov *et al.* [SAGE Collaboration], Phys. Rev. **C59** (1999) 2246-2263. [hep-ph/9803418].
F. Kaether, W. Hampel, G. Heusser, J. Kiko and T. Kirsten, Phys. Lett. B **685** (2010) 47 [arXiv:1001.2731 [hep-ex]].
- [5] C. Giunti, M. Laveder, [arXiv:1006.3244 [hep-ph]].
- [6] J. Kopp, M. Maltoni, T. Schwetz, [arXiv:1103.4570 [hep-ph]].
- [7] U. Seljak, A. Slosar and P. McDonald, JCAP **0610** (2006) 014 [arXiv:astro-ph/0604335].
E. Komatsu *et al.*, arXiv:1001.4538 [astro-ph.CO].
J. Dunkley *et al.*, arXiv:1009.0866 [astro-ph.CO].
J. Hamann, S. Hannestad, G. G. Raffelt, I. Tamborra and Y. Y. Y. Wong, Phys. Rev. Lett. **105** (2010) 181301 [arXiv:1006.5276 [hep-ph]].
- [8] Y. I. Izotov and T. X. Thuan, Astrophys. J. **710** (2010) L67 [arXiv:1001.4440 [astro-ph.CO]].
G. Steigman, JCAP **1004** (2010) 029 [arXiv:1002.3604 [astro-ph.CO]].
E. Aver, K. A. Olive and E. D. Skillman, JCAP **1005** (2010) 003 [arXiv:1001.5218 [astro-ph.CO]]; arXiv:1012.2385 [astro-ph.CO].
- [9] E. Giusarma, M. Corsi, M. Archidiacono, R. de Putter, A. Melchiorri, O. Mena, S. Pandolfi, [arXiv:1102.4774 [astro-ph.CO]].

- [10] H. Nunokawa, O. L. G. Peres and R. Zukanovich Funchal, Phys. Lett. B **562** (2003) 279 [arXiv:hep-ph/0302039].
- [11] S. Choubey, JHEP **0712** (2007) 014 [arXiv:0709.1937 [hep-ph]].
- [12] R. Abbasi *et al.* [IceCube Collaboration], Phys. Rev. D **79** (2009) 102005 [arXiv:0902.0675 [astro-ph.HE]].
- [13] R. Abbasi *et al.* [IceCube Collaboration], Phys. Rev. D **83** (2011) 012001 [arXiv:1010.3980 [astro-ph.HE]].
- [14] S. Desai *et al.* [Super-Kamiokande Collaboration], Astropart. Phys. **29** (2008) 42-54. [arXiv:0711.0053 [hep-ex]].
- [15] C. Giunti, Y. F. Li, Phys. Rev. **D80** (2009) 113007, [arXiv:0910.5856 [hep-ph]].
- [16] O. L. G. Peres, A. Y. Smirnov, Nucl. Phys. **B599** (2001) 3, [hep-ph/0011054].
- [17] A. M. Dziewonski and D. L. Anderson, Phys. Earth Planet. Interiors **25** (1981) 297.
- [18] Q. Y. Liu, A. Y. Smirnov, Nucl. Phys. **B524** (1998) 505-523. [hep-ph/9712493].
Q. Y. Liu, S. P. Mikheyev, A. Y. Smirnov, Phys. Lett. **B440** (1998) 319-326. [hep-ph/9803415].
- [19] S. Razzaque and A Yu Smirnov, paper in preparation.
- [20] P. Adamson, *et al.* [The MINOS Collaboration], Phys. Rev. **D81** (2010) 052004 [arXiv:1001.0336[hep-ex]].
- [21] P. Adamson *et al.* [MINOS Collaboration], arXiv:1104.3922 [hep-ex].

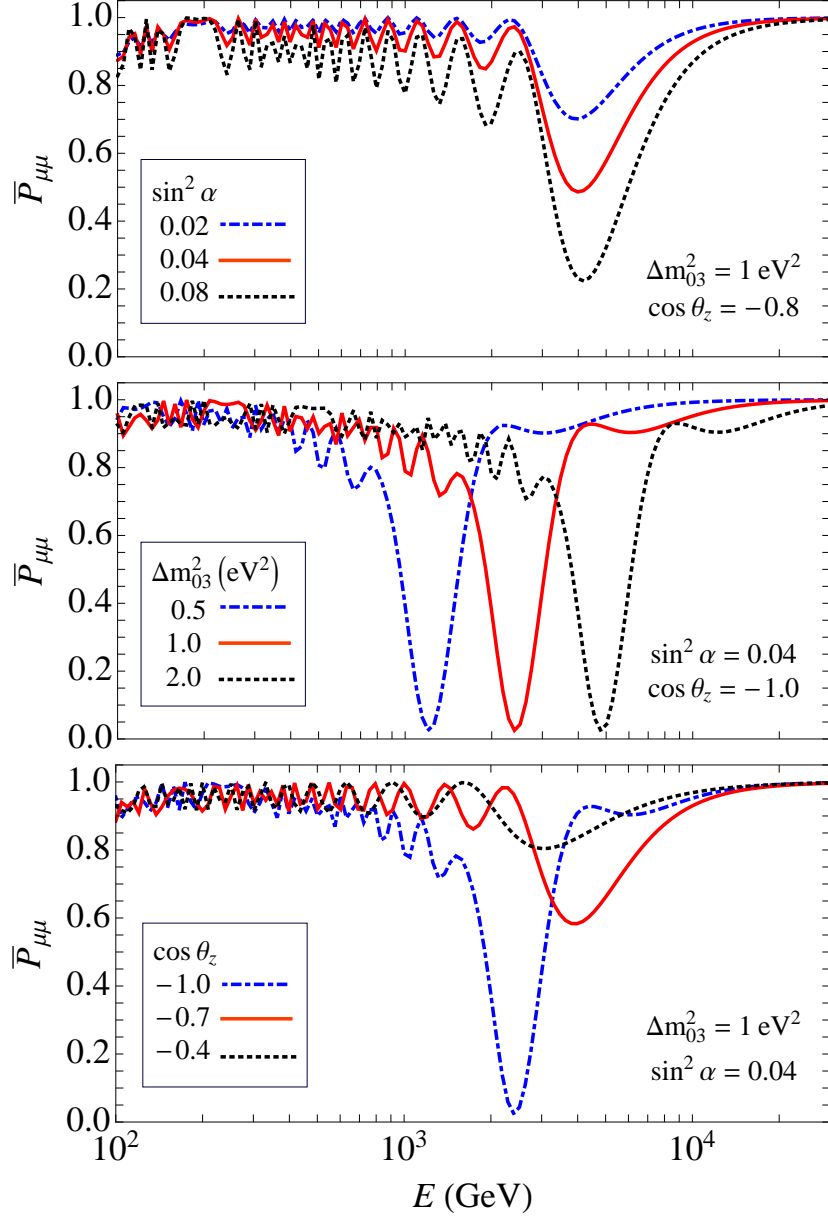


Figure 1: The survival probability of the muon antineutrinos (resonance channel) as function of the neutrino energy for different values of the zenith angle ($\cos \theta_z$) and oscillation parameters ($\Delta m_{03}^2, \sin^2 \alpha$).

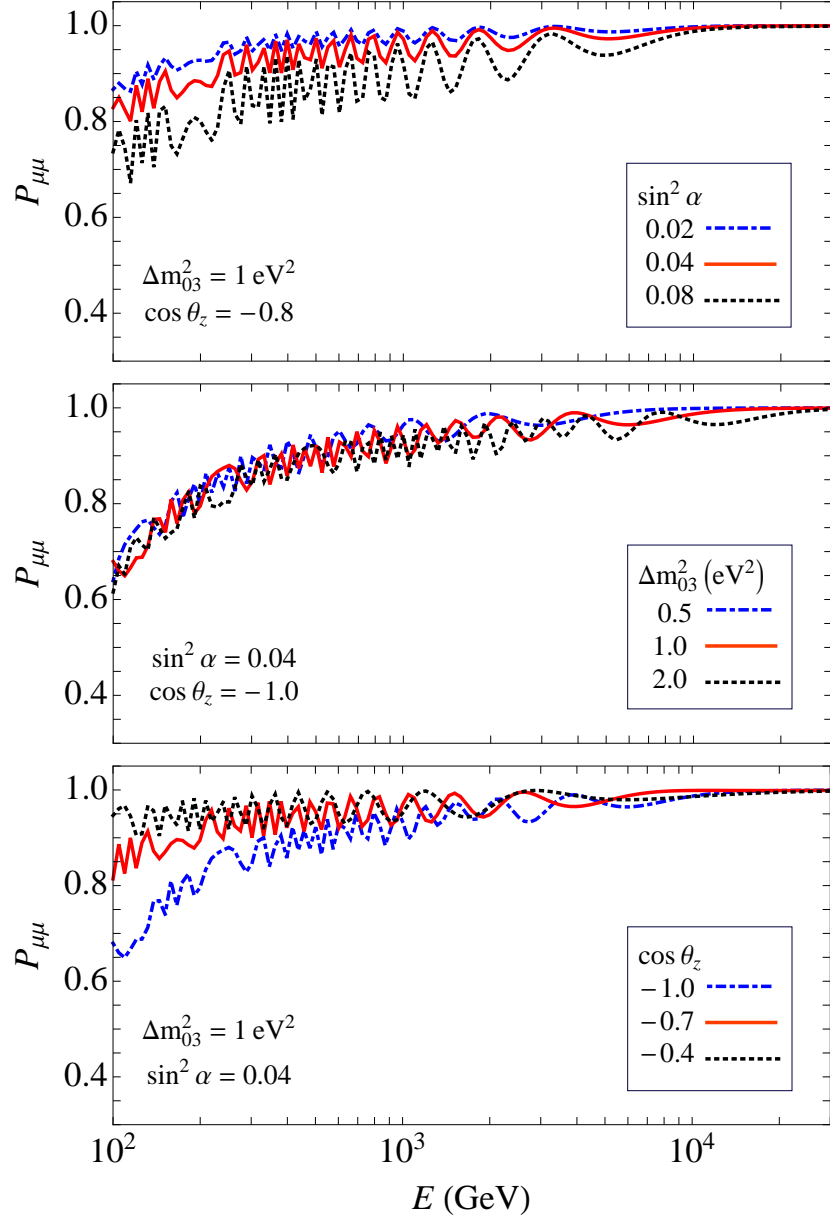


Figure 2: The same as in Fig. 1 for muon neutrinos.

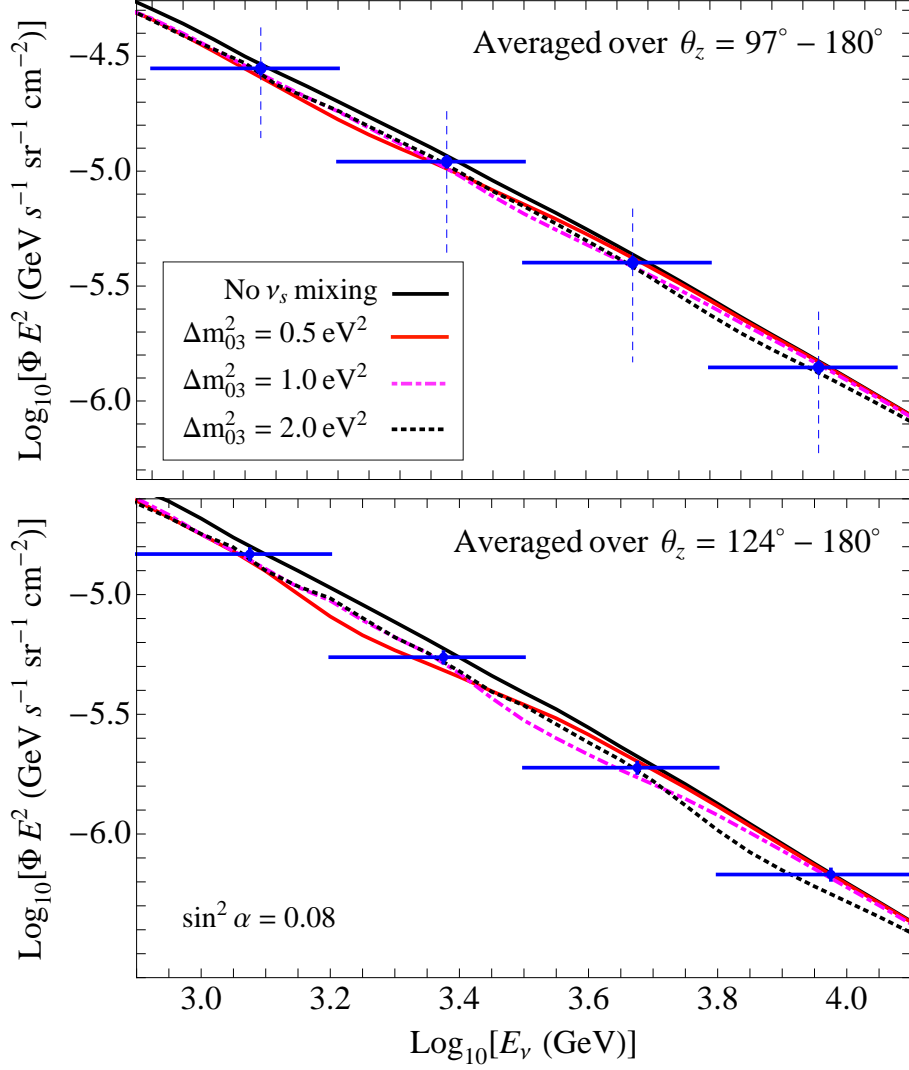


Figure 3: The energy spectrum of ν_μ integrated over the zenith angles in the intervals $97^\circ - 180^\circ$ and $124^\circ - 180^\circ$ with and without oscillations to sterile neutrinos versus IceCube result. We use the ν_s -mass mixing scheme with $\sin^2 \alpha = 0.08$ and $\Delta m_{03}^2 = 1 \text{ eV}^2$. In the top panel, the error bars denoted by the dashed lines include both statistical and systematic errors as reported by Icecube (Table II in [13]). In the lower panels, statistical-only error bars are denoted by solid vertical lines. For the top panel, the statistical error bars are about the same size as the points.

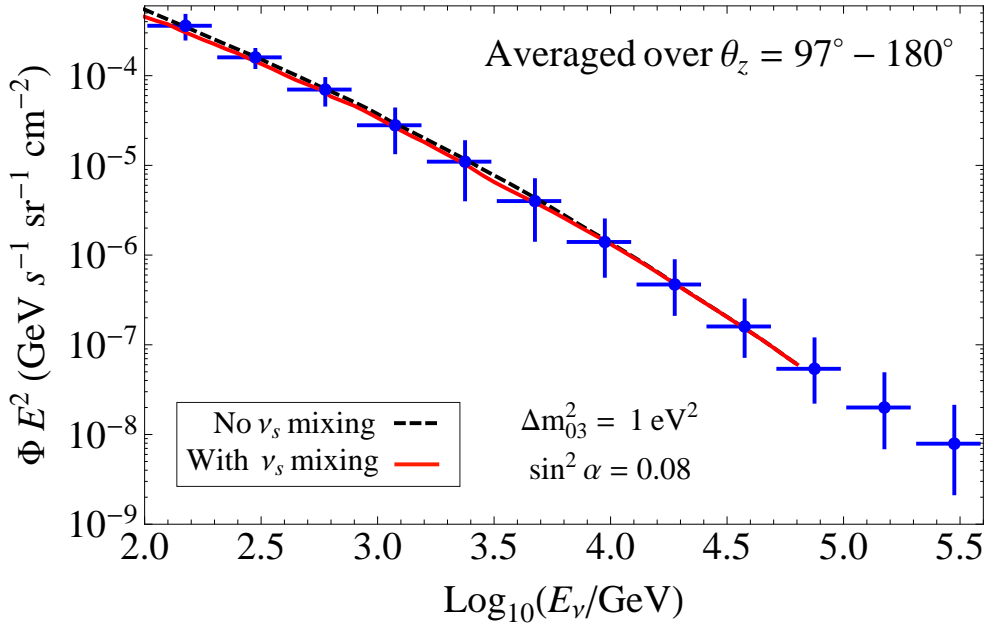


Figure 4: The ν_μ energy spectrum integrated over the zenith angle with and without oscillations to sterile neutrinos versus the IceCube results. We use $\sin^2 \alpha = 0.08$ and $\Delta m_{03}^2 = 1 \text{ eV}^2$.

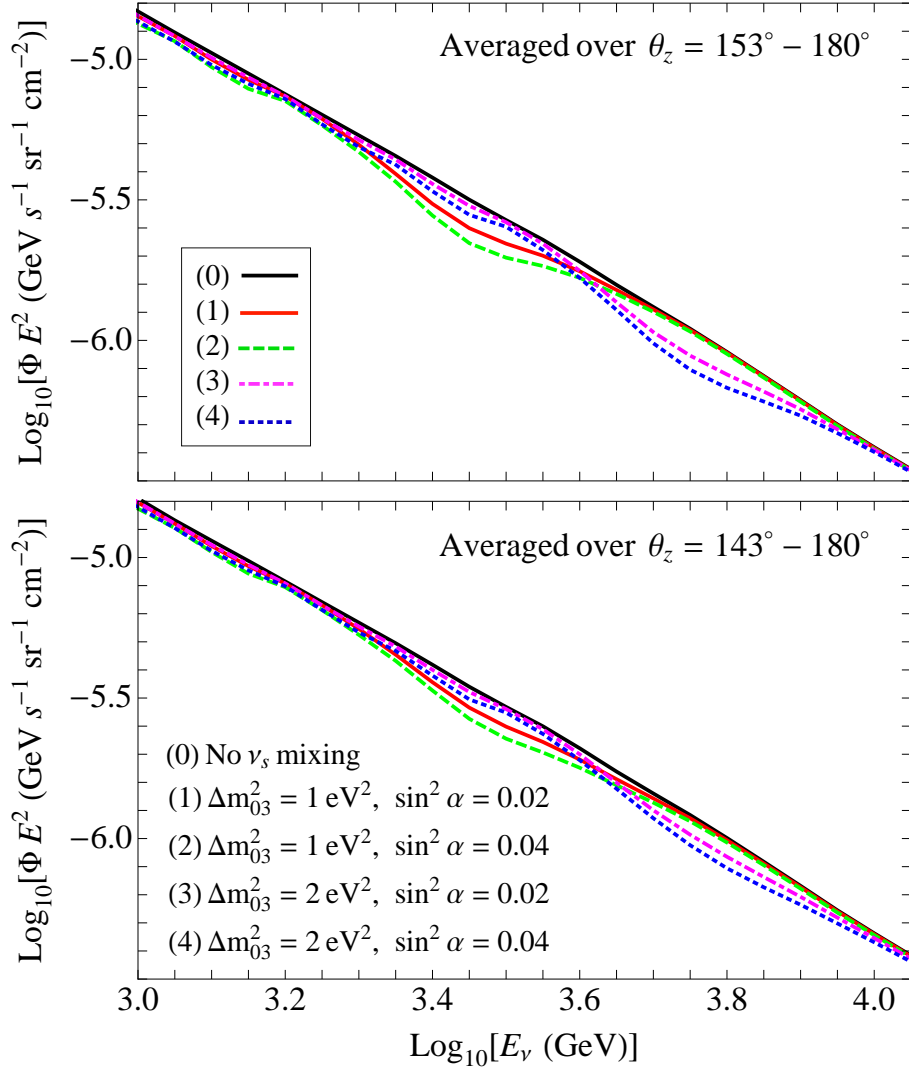


Figure 5: The ν_μ energy spectrum integrated over different intervals of zenith angles for different values of $\sin^2 \alpha$ and Δm_{03}^2 .

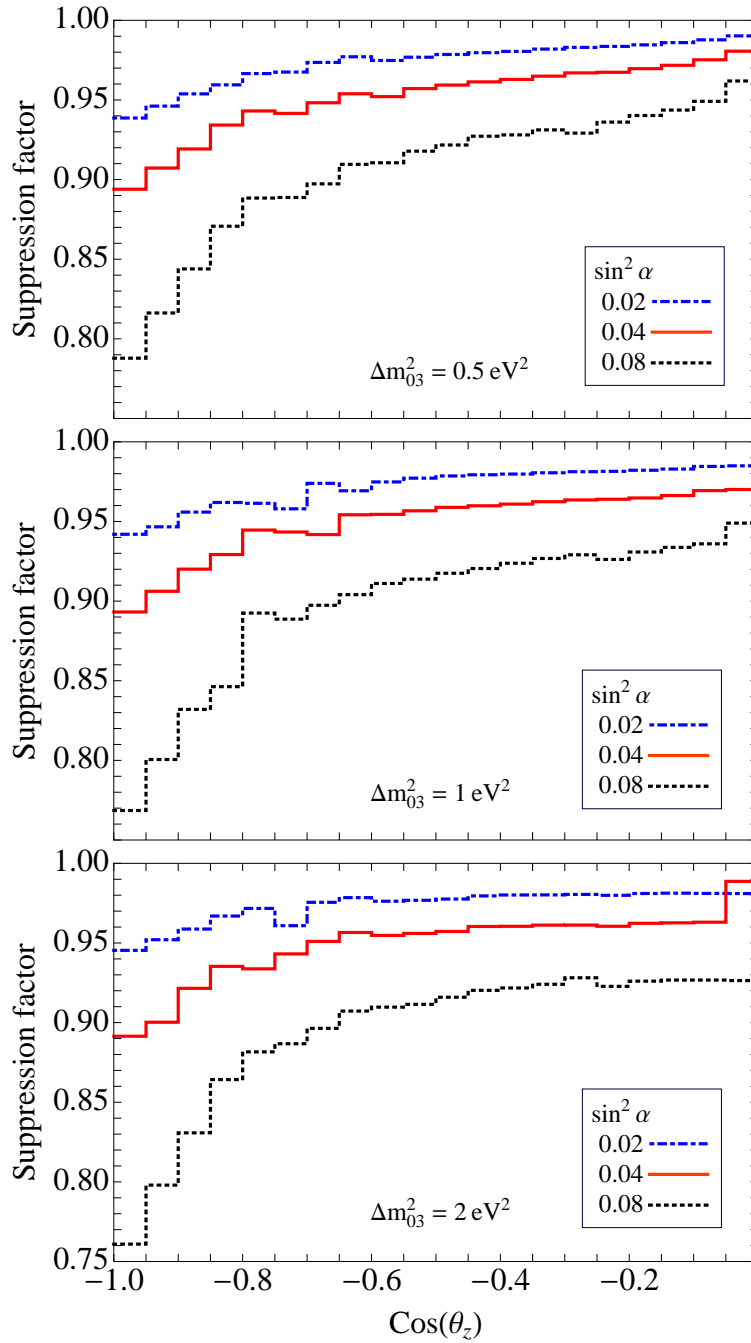


Figure 6: The zenith angle dependence of the suppression factor of the muon events integrated over the energy from $E_{th} = 0.1 \text{ TeV}$. We use the ν_s -mass mixing scheme.

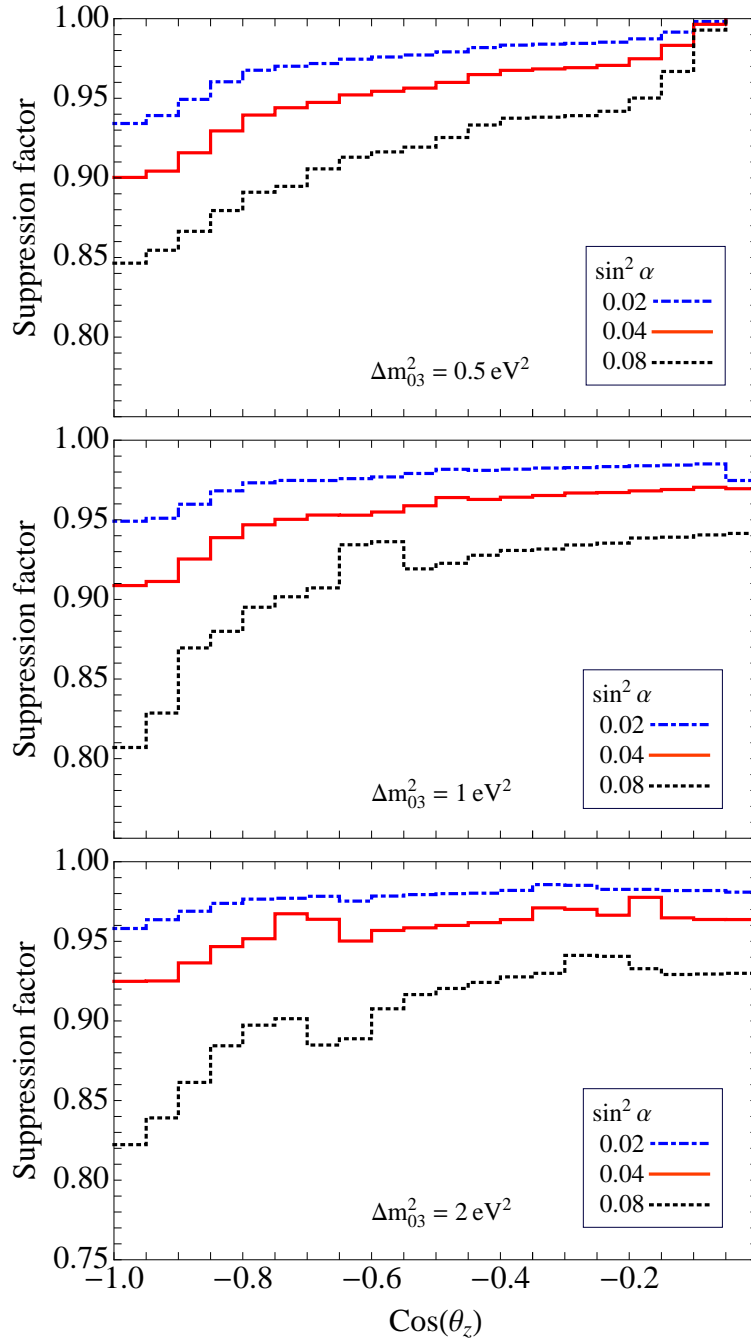


Figure 7: The same as in fig. 6 for $E_{th} = 1 \text{ TeV}$.

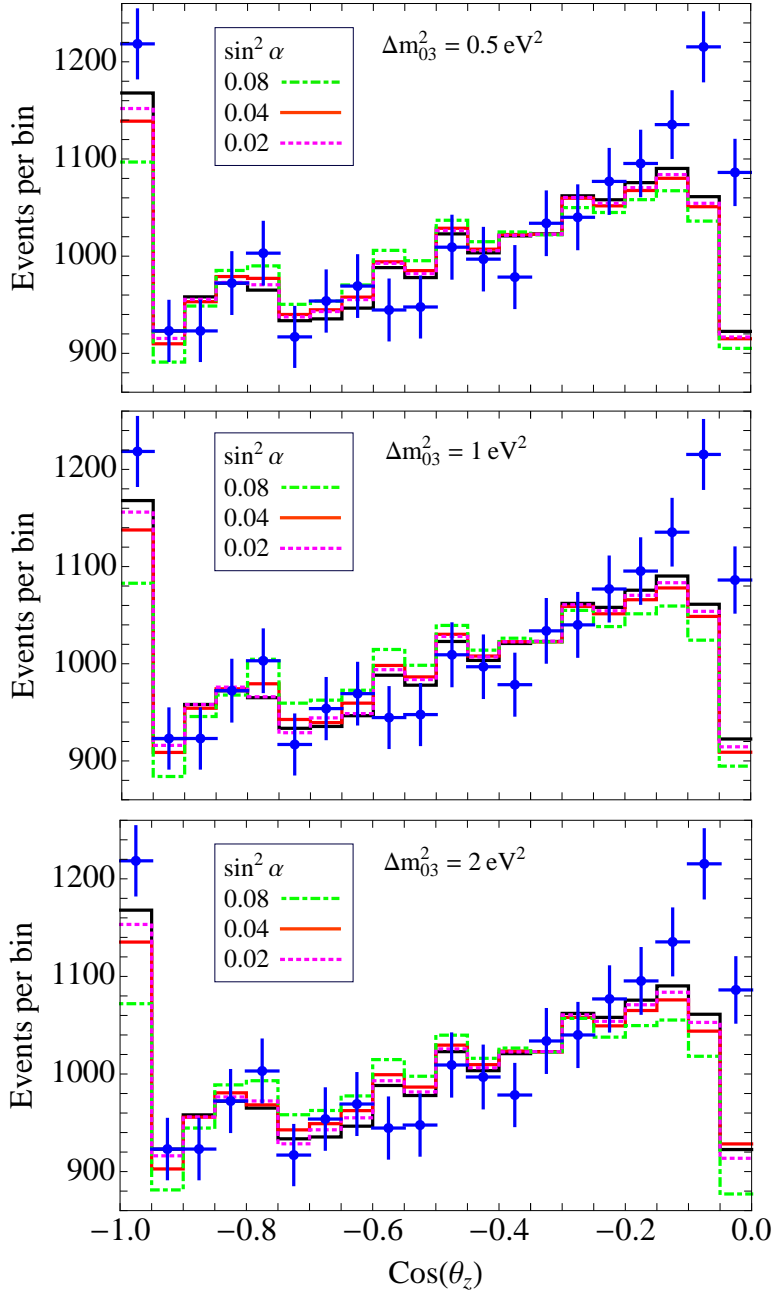


Figure 8: The zenith angle distribution of muons from ν_μ interactions integrated over the energy with and without oscillations (solid black histograms) to sterile neutrinos. We have renormalized the event distribution according to the best-fit normalization and tilt parameters from the χ^2 fit (Table 1). Also shown are the IceCube results.

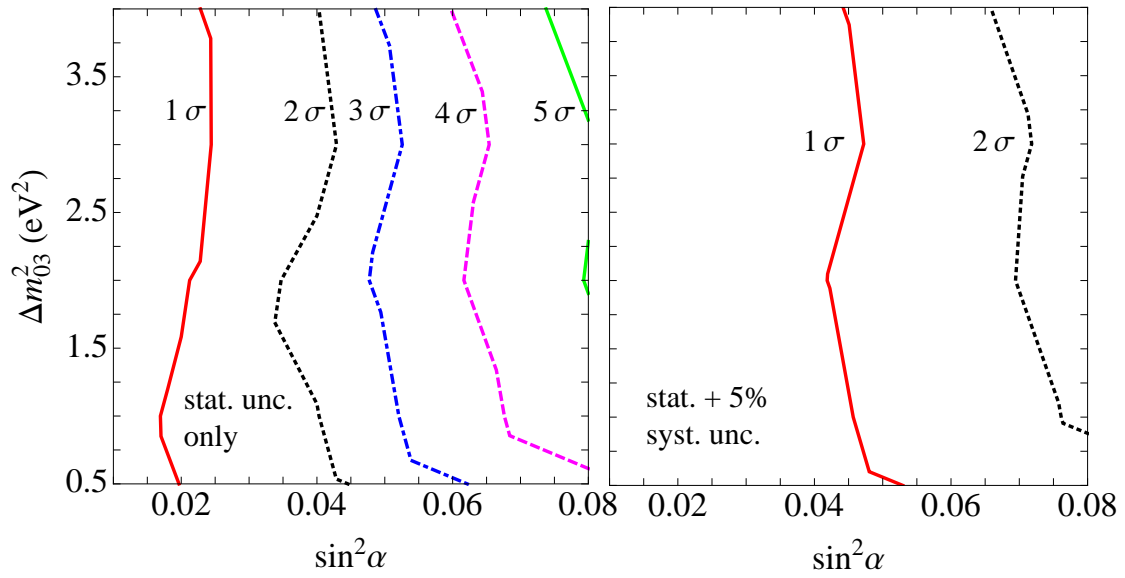


Figure 9: Bounds on the active - sterile mixing angle as function of Δm_{03}^2 obtained from the IceCube zenith angle distribution of events. Left panel - statistical errors only, right panel: statistical plus 5% uncorrelated systematic errors in each bin.

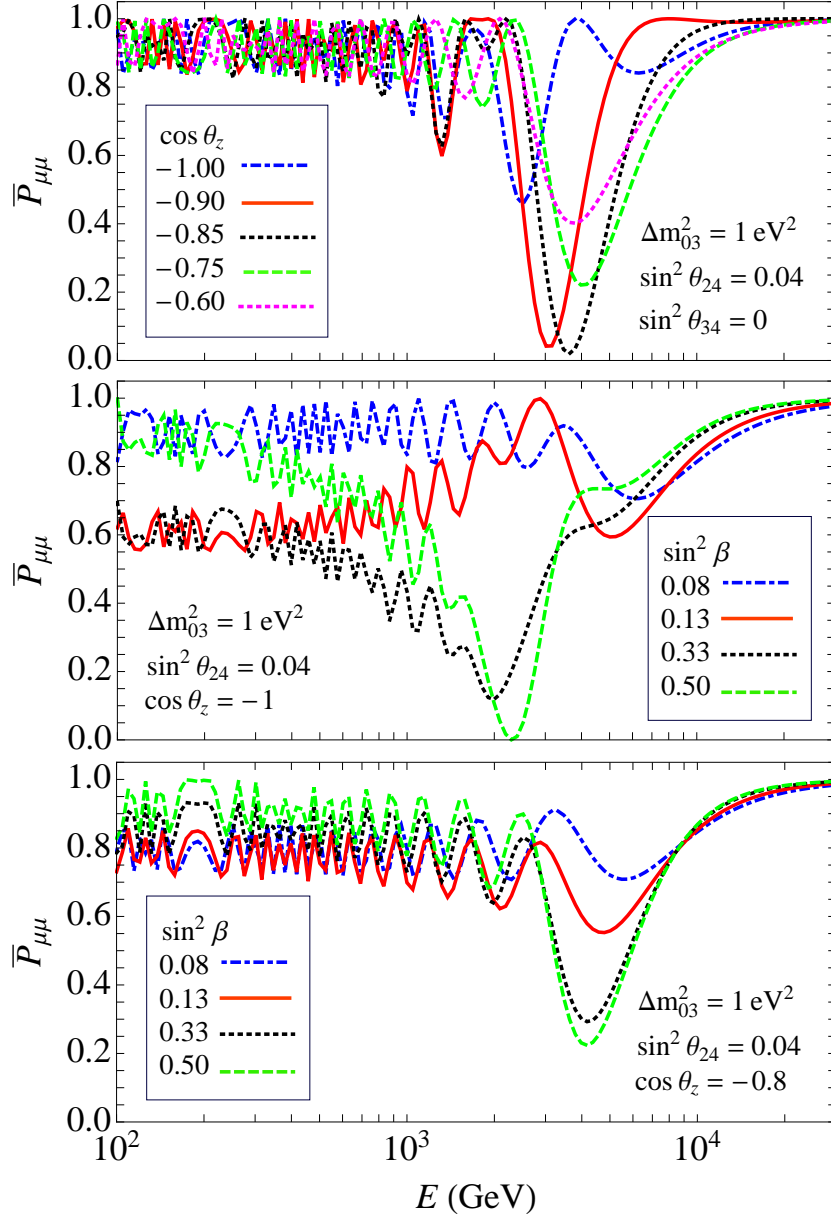


Figure 10: The survival probabilities in the antineutrino (resonance) channel as functions of neutrino energy for different mixing schemes in the leading order approximation. The *top panel* shows the probabilities for different $\cos \theta_z$ in the $\nu_\mu - \nu_s$ mixing case ($\sin^2 \beta = 0$ and $s_{34}^2 = 0$). The *middle and bottom panels* show the probabilities for different values of $\sin^2 \beta$ (s_{34}^2) and two different zenith angles, while keeping s_{24}^2 fixed.

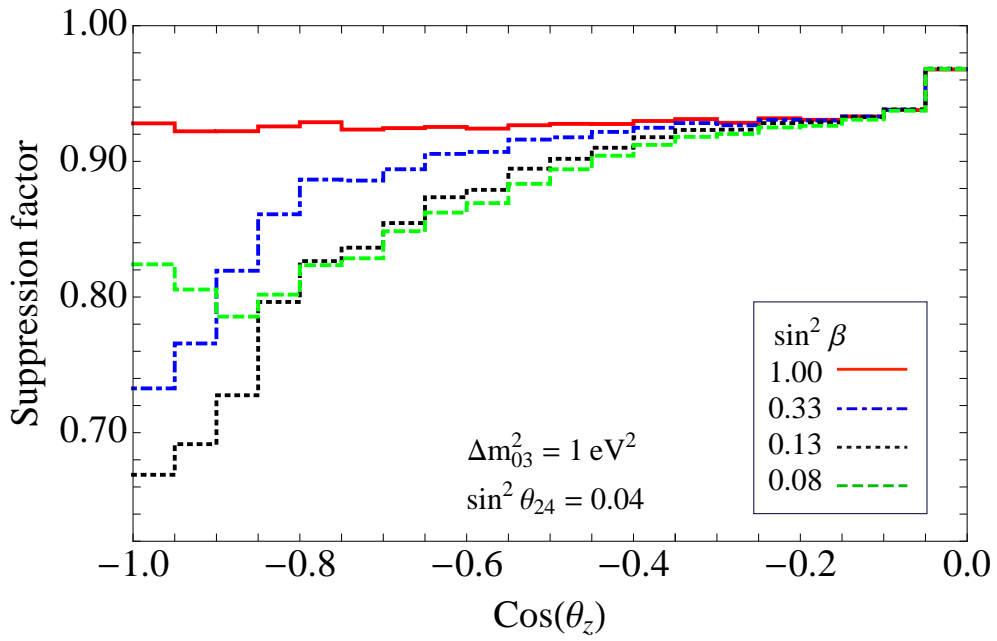


Figure 11: The suppression factor in the leading order approximation as function of the zenith angle for fixed θ_{24} and different values of $\sin^2 \beta$. We used $E_{th} = 0.1$ TeV.